Climate Dynamics
https://doi.org/10.1007/s00382-021-06119-7

The modulation of Interdecadal Pacific Oscillation and Atlantic Multidecadal Oscillation on winter Eurasian cold anomaly via the Ural blocking change

Binhe Luo[1,2] · Dehai Luo[2,3] · Aiguo Dai[4] · Ian Simmonds[5] · Lixin Wu[1]

Received: 17 April 2021 / Accepted: 22 December 2021

Abstract

Observations reveal distinct interdecadal winter Eurasian cold anomaly (ECA) centered over central Eurasia (40°–60° N, 60°–120° E), with a more southwestward extension during 1965–1976 than during 2002–2013. In this paper, Ural blockings (UB) in association with the Interdecadal Pacific Oscillation (IPO) and Atlantic Multi-decadal Oscillation (AMO) are analyzed to explain the ECA's decadal change from 1965–1976 to 2002–2013 using reanalysis data. It is found that the 1965–1976 winter ECA is associated with a negative-phase IPO (IPO^-) together with negative-phase AMO (AMO^-), while the 2002–2013 ECA is related to positive-phase AMO (AMO^+) concurring with IPO^-. UB mainly related to positive North Atlantic Oscillation is relatively short-lived and rapidly retrograde during both IPO^+ and AMO^-, but long-lived and shows different longitudinal movements and positions during IPO^- and AMO^+. During IPO^-, UB grows rapidly and decays slowly due to weak westerly winds and small meridional potential vorticity gradient (PV_y) over North Atlantic mid-high latitudes and Eurasian high latitudes, and moves slowly westward during its decay stage, causing strong cold anomalies over central Eurasia and its upstream region (30°–50° N, 30°–70° E). AMO^- has a similar effect due to the slow decay of retrograde UB. However, during AMO^+ UB grows slowly, decays rapidly and shows eastward movement due to strong (weak) westerly winds and large (small) PV_y over North Atlantic (Eurasian) high latitudes, causing strong cold anomalies over central Eurasia and its downstream side. Through these UB-induced sub-seasonal changes, the interdecadal IPO^-, AMO^- and AMO^+ help explain the decadal variation of the winter-mean ECA from 1965–1976 to 2002–2013.

1 Introduction

A pronounced feature of the recent winter air temperature variability in the Northern Hemisphere is a strong Eurasian cold anomaly (ECA) during recent winter decades around 2002–2014 (Dai and Wang 2018), which is roughly coincident with the global warming hiatus—the slowdown in the global warming rate from around 1999–2013 (Cohen et al. 2014; Mori et al. 2014; Dai et al. 2015; Wei et al. 2015; Li et al. 2015; Yao et al. 2017; Deser et al. 2017; Huang et al. 2017). A winter ECA also occurred during 1960s–1970s (Dai and Wang 2018) and thus the winter Eurasian air temperature exhibited some notable interdecadal variability (Wei et al. 2015; Huang et al. 2017; Sung et al. 2018). The interdecadal variability of the winter Eurasian air temperature has been linked to the Atlantic Multidecadal Oscillation (AMO) through the Atlantic-Eurasian wave train (Sung et al. 2018; Jin et al. 2020) and the Interdecadal Pacific Oscillation (IPO) (Dai et al. 2015). The IPO is the interdecadal variation in El Niño–Southern Oscillation (ENSO) (Dong et al. 2018), and ENSO has a significant influence on winter Ural blocking (UB, a blocking anticyclone over the Ural Mountains around 60° E and 50°–70° N that often persists for 10–20 days) and ECA (Luo et al. 2021). Thus, one might expect the IPO to have a significant impact on UB and ECA

✉ Dehai Luo
ldh@mail.iap.ac.cn

[1] Key Laboratory of Physical Oceanography/Institute for Advanced Ocean Studies, Ocean University of China and Qingdao National Laboratory for Marine Science and Technology, Qingdao, China

[2] Key Laboratory of Regional Climate-Environment for Temperate East Asia, Institute of Atmospheric Physics, Chinese Academy of Sciences, Beijing 100029, China

[3] University of Chinese Academy of Sciences, Beijing, China

[4] Department of Atmospheric and Environmental Sciences, University at Albany, SUNY, Albany, NY 12222, USA

[5] School of Earth Sciences, The University of Melbourne, Victoria, Australia

Published online: 05 January 2022

as well, even though Wu and Lin (2012), Wu and Zhang (2015) and Zhou and Wu (2016) connected the summer Eurasian heat waves to the interdecadal variability of ENSO and AMO and the positive phase of AMO can have an important impact on the shape of UB (Luo et al. 2017b).

It has been recognized that UB's longitudinal location, movement and persistence are more important for the occurrence region and strength of the sub-seasonal ECA over central Eurasia than the strength of blocking itself (Yao et al. 2017). In contrast, the European blocking and Atlantic blocking are not important for the cold anomaly over central Eurasia (Luo et al. 2019a, b, c). While UB is linked to sea ice loss in the Barents–Kara Seas (BKS) (Mori et al. 2014; Yao et al. 2017; Li et al. 2021), Euro-Atlantic blocking and UB are also modulated by AMO (Rimbu et al. 2014; Luo et al. 2017a, b; Chen et al. 2021). However, it is unclear how the IPO and AMO might influence the winter ECA through their modulation of UB, as the sub-seasonal ECA is closely related to the presence of UB (Luo et al. 2016a, b; Yao et al. 2017; Tyrlis et al. 2020; Kim et al. 2021), and what are the different roles the IPO and AMO play in the winter ECA. Moreover, how UB's position, movement and evolution (i.e., growth and decay) change with the IPO and AMO, and how such UB changes influence the sub-seasonal ECA are unclear and not explored in previous studies.

As the winter-mean ECA is derived from the sub-seasonal ECA, we hypothesize that the UB-induced changes in sub-seasonal ECAs modulated by IPO and AMO may play a significant role in causing the winter decadal ECA. Here, we investigate the different behavior of UB under different phases of IPO or AMO and offer a synoptic explanation from a blocking perspective for why the spatial pattern of the winter ECA shows a distinct change from 1965–1976 to 2002–2013 (Fig. 1). We refer to this winter ECA change from 1965–1976 to 2002–2013 as the decadal change of ECA in this paper. Because the IPO and AMO are multidecadal modes, they do not directly excite UB events which have a sub-seasonal time scale ranging from 10 to 20 days. Instead, they can provide an interdecadal background condition (Wyatt et al. 2012) influencing UB. Thus, we hypothesize that the phase of IPO or AMO can contribute to the change of the winter ECA from 1965–1976 to 2002–2013 through their interdecadal modulation of UB's position, movement, evolution and persistence. Such a study can help explain the change in the spatial pattern of the winter ECA from 1965–1976 to 2002–2013, which is not revealed in previous studies (e.g., Luo et al. 2017b; Sung et al. 2018; Luo et al. 2019a, b, c; Chen et al. 2021).

This paper is arranged as follows: In Sect. 2, the data and method are described. We present the connections of the winter ECA during 1965–1976 and 2002–2013 to changes in UB events in Sect. 3. In Sect. 4, we examine how the phase of IPO or AMO modulates the sub-seasonal ECA through changing the position, movement, persistence and evolution of UB events. Section 5 examines the physical processes through which the IPO or AMO modulates UB. The summary and conclusions are presented in Sect. 6.

2 Data and method

We used the daily data on a $2.5° \times 2.5°$ grid for winter (December, January and February, DJF) during the period from December 1950/February 1951 to December 2017/February 2018 (1950–2017, hereafter) taken from National Centers for Environmental Prediction-National Center for Atmospheric Research (NCEP-NCAR) reanalysis (Kalnay et al. 1996) (https://www.esrl.noaa.gov/psd/data/gridded/data.ncep.reanalysis). They include surface air temperature (SAT), 500-hPa geopotential height (Z500) and zonal wind (U500). We also repeated the analyses using the ERA5 reanalysis (Hersbach et al., 2020) and the results are similar (see Figs. S2–3). All the daily fields were converted into anomaly fields through removing the 1950–2017 mean of each calendar day, and then detrended prior to analyses. We also used the winter monthly sea surface temperature (SST) and sea ice concentration (SIC) data on a $1° \times 1°$ grid during 1950–2017 from the HadISST1 taken from the Hadley Centre (Rayner et al. 2003) (http://www.metoffice.gov.uk/hadobs/hadisst/data/).

There are many ways to define the IPO (Dai 2013; Dong et al. 2018; Hua et al. 2018). For example, the winter IPO can be defined as the principal component (PC) of the first EOF of detrended, 3-year moving averaged DJF-mean SST from HadISST1 over 60° S–60° N (Dong and Dai 2015). Here, we used the winter IPO index obtained from the Koninklijk Nederlands Meteorologisch Instituut (KNMI) Climate Explorer (https://climexp.knmi.nl/selectindex.cgi?id=someone@somewhere). Following Trenberth and Shea (2006), the DJF-mean SST anomalies from HadISST1 averaged over 0°–60° N, 0°–80° W minus the DJF-mean SST anomalies averaged over the global oceans from 60° S to 60° N is defined as the AMO index. The winter AMO index we used here was directly taken from the KNMI Climate Explorer. Results are similar if the AMO index from Kaplan et al. (1998) is used. Below, we will use the 9-year smoothed IPO and AMO indices taken from the KNMI Climate Explorer to investigate the modulation of the IPO and AMO on UB and associated sub-seasonal ECA and explain the change of the winter ECA from 1965–1976 to 2002–2013.

Here we define a positive (negative) phase IPO or IPO^+ (IPO^-) as the year with positive (negative) value above 0.5 (below -0.5) standard deviations (STDs) for the 9-year smoothed DJF-mean IPO index. The positive (negative) phase AMO or AMO^+ (AMO^-) is similarly defined using the 9-year smoothed DJF-mean AMO index. To ensure that

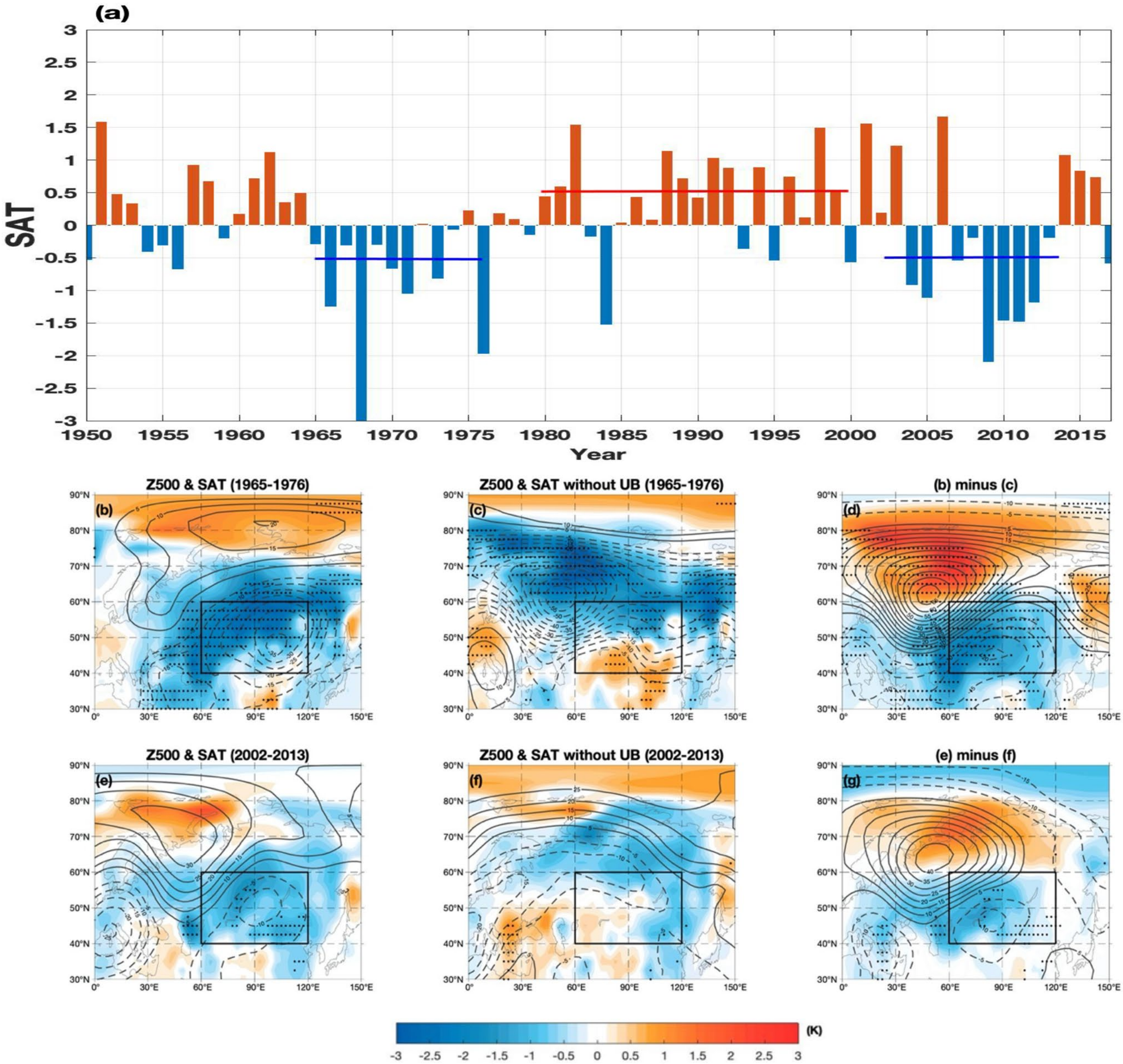

Fig. 1 **a** Time series of DJF-mean surface air temperature (SAT) anomalies averaged over central Eurasia (60°–120° E, 40°–60° N), with the red line denoting the 1980–2000 period, and the blue lines marking the 1965–1976 and 2002–2013 periods respectively. **b**–**g** DJF-mean Z500 anomalies (contours; contour interval (CI) = 5 gpm) and SAT (color shading in unit of K) anomalies averaged during **b**–**d** 1965–1976 and **e**–**g** 2002–2013 for UB events **b**, **e** included and **c**, **f** excluded (blocking days from lag − 10 to 10 days are removed, lag 0 denotes the day of the UB peak) as well as their differences: **d** b minus c and **g** e minus f. The dot represents the areas of the SAT anomaly being significant at the 95% level based on a two-sided Student t-test. Black box represents the central Eurasia or Siberia, which has the same meaning as below

there are enough winters of the different IPO and AMO (IPO/AMO) phase combinations, we used the zero threshold to define the IPO/AMO phase combination. As in Huang et al. (2019), an IPO^- and AMO^- (or IPO^-/AMO^-) combination winter is defined if their 9-year smoothed indices are negative, whereas an IPO^- and AMO^+ (or IPO^-/AMO^+) combination winter is defined if the 9-year smoothed IPO (AMO) index is negative (positive). The other combination winters are similarly defined. The results based on the 0.5 STD threshold are similar (not shown).

To identify UB events in the Ural Mountains region around 60° E, the one-dimensional (1D) blocking index by Tibaldi and Molteni (1990, TM hereafter) is used to calculate UB events over the region 40°–80° E. The TM index is established based on the reversal of the meridional gradients of Z500: $GHGN = \frac{Z500(\phi_N) - Z500(\phi_o)}{\phi_N - \phi_o}$ and $GHGS = \frac{Z500(\phi_o) - Z500(\phi_S)}{\phi_o - \phi_S}$ at three given latitudes $\phi_N = 80^\circ N + \Delta$, $\phi_o = 60^\circ N + \Delta$, $\phi_S = 40^\circ N + \Delta$ and $\Delta = -5^\circ, 5^\circ, 5^\circ$. A blocking event is defined to have taken place in a given region if both $GHGS > 0$ and $GHGN < -10$ gpm (deg lat)$^{-1}$ persist at least three consecutive days and are satisfied for at least one choice of Δ in the zonal domain of 15° longitudes. At the same time, the duration of UB is estimated by calculating the consecutive days with the daily Z500 anomaly averaged over the blocking latitude band (50°–70° N) exceeding a threshold of 80 gpm, and used to represent the local persistence time of the UB in the Ural region as in Luo et al. (2018). The change speed of the daily zonal location of the maximum anticyclonic anomaly averaged over 50°–70° N is defined as the daily phase speed of UB, whereas its time-mean value averaged over the blocking duration confined in the Ural region is defined as the mean movement speed of UB. In our composite, the day of the GHGS peak is defined as lag 0 of UB (Luo et al. 2017a, b).

Diao et al. (2006) evaluated the different blocking indices in identifying the blocking action in the Northern Hemisphere and demonstrated that the 1D TM index is an appropriate metric for identifying blocking events over the Ural region. We compared different blocking indices (e.g., the 1D TM index and the PV-θ index in Masato et al. 2013 and Woollings et al. 2008) and found that UB events and their durations are not very sensitive to the choice of the blocking index (Luo et al. 2018; Tyrlis et al. 2020). Thus, in this paper we use only the 1D TM index to identify UB events.

Our daily North Atlantic Oscillation (NAO) index was taken from the NOAA/Climate Prediction Center (https://www.cpc.noaa.gov/products/precip/CWlink/pna/nao.shtml). We also define a positive (negative) NAO or NAO^+ (NAO^-) event to have happened if the daily NAO index is equal to or above 0.5 (below -0.5) STDs with at least three consecutive days. We define other daily events that are neither an individual NAO^+ nor NAO^- event as neutral NAO (NAO°) events. UB events associated with the NAO^+ (NAO^-) event are referred to as the UB-NAO^+ (UB-NAO^-) events if the peak of the GHGS associated with UB takes place within the life cycle of the NAO^+ (NAO^-) event (e.g., Luo et al. 2017a). UB event with NAO° is referred to as the UB-NAO° event.

We used the two-sided Student t-test for determining the statistical significance of the anomaly field at each grid point or the difference between two types of anomaly fields, but use the Monte Carlo test (using 5000 simulations generated by repeated random sampling) to examine the statistical significance for the difference between two time series or between two duration lengths. Both tests are conducted at the $p < 0.05$ level. These methods are described in Wilks (2011).

As demonstrated theoretically by Luo et al. (2019b) and Zhang and Luo (2020), the magnitude of the meridional gradient (PV_y) of the potential vorticity (PV) is a key factor influencing the behavior (duration, movement and evolution) of atmospheric blocking. The non-dimensional PV_y at 500 hPa is defined as $PV_y = \beta - \frac{\partial^2 U500}{\partial y^2} + FU500$ ($F \approx 1$ for a barotropic atmosphere and β is the non-dimensional north–south gradient of the Coriolis parameter f), and U500 is the non-dimensional basic westerly wind at 500 hPa, which can be directly calculated using non-dimensional DJF-mean 500-hPa zonal wind fields for blocking events excluded. When PV_y is small in the blocking region, atmospheric blocking has weak energy dispersion and strong nonlinearity such that it can have a long lifetime (Luo et al. 2019b). The strength of the upstream zonal wind or PV_y is important for whether the blocking shows different evolution (growth and decay) (Zhang and Luo 2020) and movement (Yao et al. 2017). When the upstream westerly wind or PV_y is weak, the atmospheric blocking exhibits rapid growth and slow decay. The reverse is seen for a strong upstream westerly wind or a large upstream PV_y (Zhang and Luo 2020). Below, we will use these insights to explain why the IPO or AMO can influence the persistence, movement and evolution of UB and their different impacts on Eurasian SAT anomalies by examining the changes in DJF-mean westerly wind and PV_y related to the phase of IPO or AMO.

3 Decadal Eurasian cold anomalies and their linkage to UB events

It is useful to first show the time series of DJF-mean SAT anomalies averaged over central Eurasia (40°–60° N, 60°–120° E; CE) or Siberia from December 1950 to February 2018 (1950–2017) in Fig. 1a, with the DJF-mean Z500 and SAT anomaly patterns for 1965–1976 and 2002–2013 shown in Figs. 1b, e. Although the SAT anomaly over CE is positive for 2002–2003 (Fig. 1a), we included them in the recent ECA period in order to have the same time length sampling for the two decadal periods. The composite Z500 and SAT anomalies using only 2004–2013 (Fig. S1b in the supplementary file) are similar to those for 2002–2013 (Figs. 1b). The cold anomaly is stronger over Eurasia and extends more to the west and south of CE during 1965–1976 (Fig. 1b) than during 2002–2013 (Fig. 1e). Such a large change of the winter ECA from 1965–1976 to 2002–2013 was not noted in previous studies (Luo et al. 2017b; Sung et al. 2018; Jin et al. 2020; Chen et al. 2021). When the UB events (i.e., the blocking days ranging from lag −10 to 10 days with lag 0 denoting the day of the UB peak) and associated sub-seasonal ECAs are removed from the DJF-mean Z500 and SAT fields, the winter ECAs become much weaker in the south of 60°N for both 1965–1976 (Fig. 1c) and 2002–2013 (Fig. 1f) than those with UB events (Fig. 1b, e). In this case, the significant cold anomaly is mainly located north of 60° N for 1965–1976 (Fig. 1c), whereas the 2002–2013 ECA is almost insignificant over CE and has a weak cold anomaly east of 100° E (Fig. 1f).

Our calculations show that the domain-averaged SAT anomaly over CE is −1.47 K for 1965–1976 (Fig. 1b) and −0.86 K for 2002–2013 (Fig. 1e), but it becomes −0.4 K for 1965–1976 (Fig. 1c) and −0.3 K for 2002–2013 (Fig. 1f) when the UB days are excluded (i.e., the days from lag −10 to 10 days of each UB event are removed from the composite averaging). As a result, the UB events contribute ~73% during 1965–1976 and ~65% during 2002–2013 to the winter ECA. The rest of the winter ECA may be related to the direct impacts on winter Eurasian SAT by IPO and AMO (not via UB) or other decadal changes. Thus, the presence of UB has a significant contribution to the winter ECAs during 1965–1976 and 2002–2013. The differences of DJF-mean Z500 and SAT anomalies between the cases with and without UBs reflect the role of UB in the winter ECAs during 1965–1976 (Fig. 1d) and 2002–2013 (Fig. 1g). We note that the winter cold anomaly associated with UBs in the upstream region of CE is stronger during 1965–1976 (Fig. 1d) than during 2002–2013 (Fig. 1g). As noted below, the change of the UB-induced SAT anomaly from 1965–1976 to 2002–2013 is weaker over the downstream side of CE than over its upstream side.

We further show the 1965–1976 minus 2002–2013 difference fields for DJF-mean Z500 and SAT anomalies in Fig. 2 for the two cases with and without UB. Figure 2a shows that a strong cold anomaly difference appears mainly to the south of 60° N and in the upstream region of CE. Such a cold anomaly difference is relatively weak for the case without UB (Fig. 2b). The 1965–1976 minus 2002–2013 difference of the DJF-mean SAT anomaly averaged over EC is about −0.6 K for the case with UB, but decreases to −0.1 K for the case without UB. Moreover, the DJF-mean SAT differences averaged over the upstream region (30°–50° N, 30°–70° E) and the downstream region (30°–50° N, 90°–130° E) are −0.88 K and 0.15 K (−0.33 K and 0.53 K) respectively, for the case with (without) UB. Thus, one can infer that the decadal difference of the winter ECA is related to the variability of UB from 1965–1976 to 2002–2013. These results also hold for the ERA5 data (Figs. S2, S3), even though the details of the winter ECA patterns are slightly different. Although the NAO^+ and NAO^- events without UB can influence the winter SAT anomaly over Eurasia (Luo et al. 2016b), they cannot produce cold anomalies over central Eurasia or Siberia south of 60°N (Fig. S4). Thus, in the following discussions we do not discuss the roles of NAO^+ and NAO^- events without UB, but instead we examine the role of UB in the sub-seasonal ECA.

We first show the time series of the number of UB events in winter during 1950–2017 in Fig. 3a to examine whether UB events exhibit a notable variation between 1965–1976

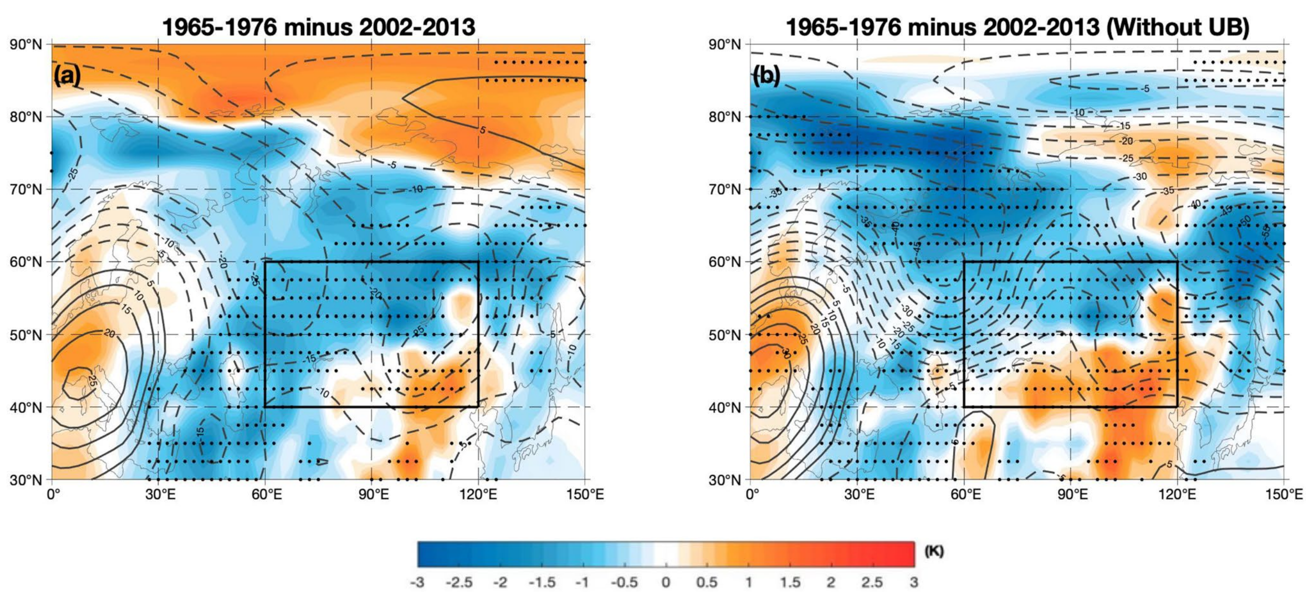

Fig. 2 The 1965–1976 minus 2002–2013 difference fields of DJF-mean Z500 (contours, CI = 5 gpm) and SAT (color shading in unit of K) anomalies for the cases **a** with and **b** without UB. The dot represents the SAT anomaly region being significant at the 95% level based on a two-sided Student t-test

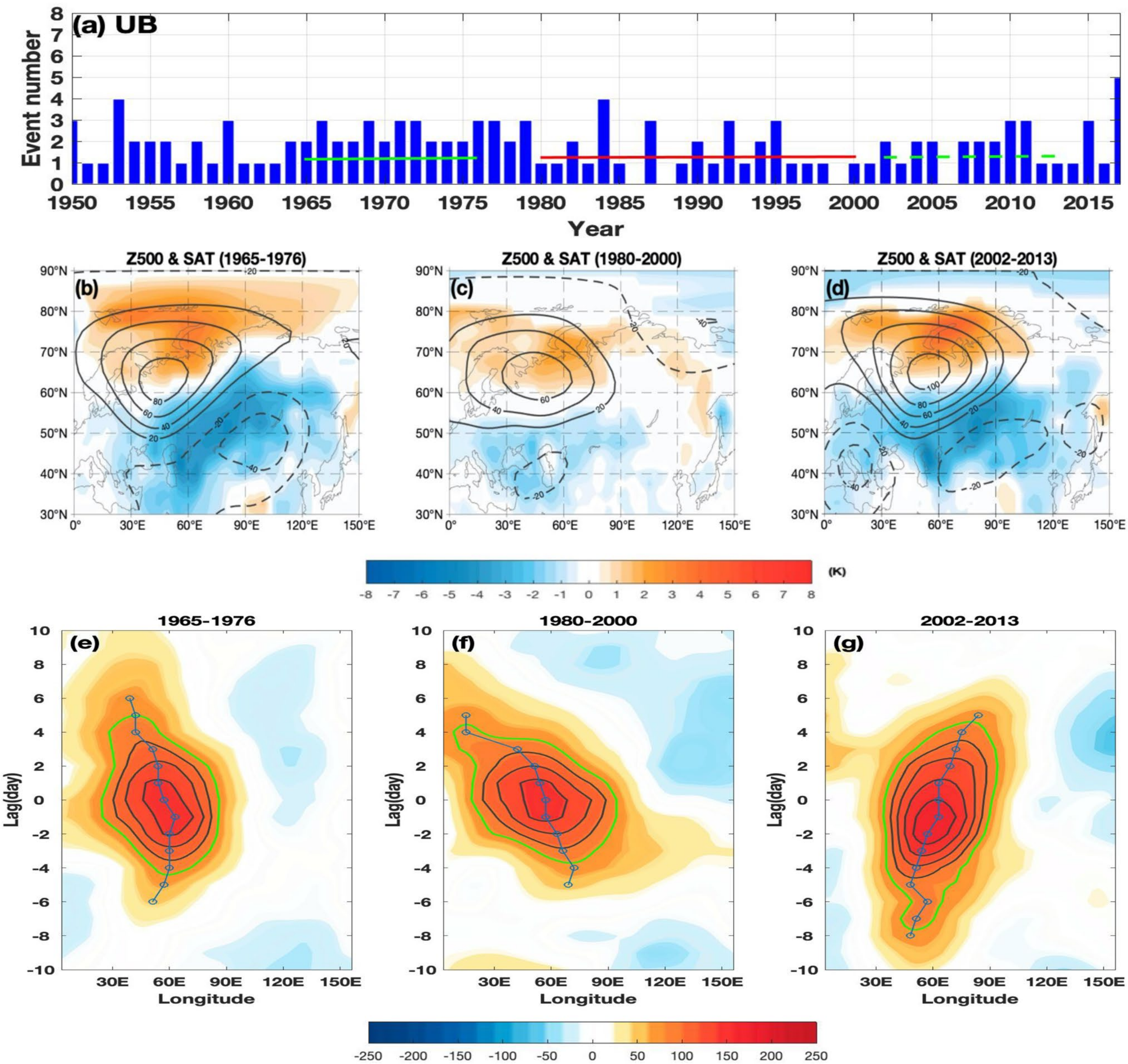

Fig. 3 **a** Time series of the number of winter Ural blocking (UB) events (a total of 126 cases) during 1950–2017 with three sub-periods: 1965–1976 (29 cases, blue line), 1980–2000 (30 cases; red line) and 2002–2013 (21 cases; dashed green line). **b**–**d** Time-mean composite daily Z500 (contours, CI = 20 gpm) and SAT (color shading, unit in K) anomalies averaged from lag − 10 to 10 days (lag 0 denotes the peak day of blocking) for **b** 29 UB events during 1965–1976, **c** 30 UB events during 1980–2000 and **d** 21 UB events during 2002–2013. **e**–**g** Time-longitude evolution of the composite daily Z500 anomalies (unit: gpm and CI = 20 gpm) averaged over 50°–70° N of the UB events during **e** 1965–1976, **f** 1980–2000 and **g** 2002–2013. In **e**–**g**, the 80 gpm contour is marked by the green line and the thick blue line denotes the zonal location of the maximum daily Z500 anomaly whose temporal variation represents the movement speed. In panels **b**–**d**, the color shading represents the SAT anomaly region being significant at the 95% confidence level based on a two-sided Student *t*-test

and 2002–2013. Figure 3a shows that there are 29, 30 and 21 UB events (or 2.42, 1.43, and 1.75 UB events per winter) during 1965–1976, 1980–2000, and 2002–2013, respectively. The difference of the UB event frequency between 1965–1976 and 2002–2013 is statistically insignificant at the 90% confidence level based on a Monte-Carlo test. Thus, the decadal variation of the winter UB event frequency cannot explain the Eurasian SAT change from 1965–1976 to 2002–2013.

To further understand the mechanisms behind this SAT change, we show the time-mean fields of composite daily Z500 and SAT anomalies averaged from lag -10 to

10 days of UB events in Fig. 3b–d for three decadal epochs: 1965–1976, 1980–2000 and 2002–2013. Correspondingly, the time-longitude plots of composite daily Z500 anomalies averaged over 50°–70° N during the UB life cycle are presented in Fig. 3e–g. It is found that while the strong Eurasian cold anomalies mainly over central Eurasia during both 1965–1976 and 2002–2013 (Fig. 3b, d) are associated with long-lived UB events having the durations of about 9–11 days (Fig. 3e, g) that satisfy the 80 gpm threshold of the UB amplitude as defined in Sect. 2, the sub-seasonal ECA extends more to the southwest and covers a wider region in 1965–1976 (Fig. 3b) than in 2002–2013 (Fig. 3d). The time-mean UB is centered at (45° E, 62° N) during 1965–1976, but at (52° E, 65° N) during 2002–2013; thus, the time-mean UB is located more west during 1965–1976 than during 2002–2013. Moreover, we see that the time-mean sub-seasonal ECAs during 1965–1976 (Fig. 3b) and 2002–2013 (Fig. 3d) also resemble the DJF-mean SAT anomalies of UB events (Fig.1d, g), even though the sub-seasonal ECA pattern in 2002–2013 (Fig. 3d) has a small difference with the DJF-mean result in Fig. 1g. It is further seen that UB moves westward especially during the decaying phase and grows rapidly but decays slowly during 1965–1976 (Fig. 3e), whereas it moves eastward and grows slowly but decays rapidly during 2002–2013 (Fig. 3g). Thus, it is inferred that the difference of the sub-seasonal ECA between 1965–1976 and 2002–2013 is related to the difference of UB in longitudinal position, movement and evolution, as noted below.

It is further seen that the upstream enhancement of the sub-seasonal ECA during 1965–1976 (Fig. 3b) is likely related to the westward movement, rapid growth and slow decay of long-lived UB (Fig. 3e) through the enhanced upstream cold temperature advection associated with low-level winds (Fig. S5a) (Yao et al. 2017). This reflects that UBs during 1965–1976 mainly influence the central Eurasia and its upstream region. In contrast, the enhanced sub-seasonal cold anomaly over CE and in the downstream region (Fig. 3d) during 2002–2013 is linked to the eastward movement, slow growth and rapid decay of long-lived UBs (Fig. 3g) due to enhanced downstream cold temperature advection (Fig. S5c) associated with the eastward movement of UB. Because UBs have a shorter duration and move rapidly westward during 1980–2000 (Fig. 3f), the Eurasian warm anomaly during 1980–2000 is likely related to short-lived, rapidly retrograde UB events and weak cold advection (Fig. S5b) during this period. We note here that we do not investigate the changes of Eurasian air temperatures from 1965–1976 to 1980–2000 or from 1980–2000 to 2002–2013, as our emphasis is on the exploration of the physical cause of the interdecadal change of the winter ECA from 1965–1976 to 2002–2013.

Our calculations show that UB possesses a longer duration of nearly 9 days (11 days) over 40°–80° E with a movement speed of about − 1.4 m/s (1.6 m/s) during 1965–1976 (2002–2013) (Figs. 3e, g) than that of about 7 days with a large retrogression speed of about − 2.2 m/s during 1980–2000 (Fig. 3f). While the UB's duration difference between 1965–1976 and 2002–2013 is not statistically significant according to a Monte-Carlo test, UB shows opposite movement and evolution (growth and decay) between the two periods. Thus, the difference of the winter ECA spatial patterns between 1965–1976 (Fig. 1b) and 2002–2013 (Fig. 1c) is mainly related to the different longitudinal position, movement and evolution of long-lived UBs in the two periods (Fig. 3e, g). These findings are not reported in our previous studies (Luo et al. 2017b; Chen et al. 2021).

We now examine whether the change of the UB-related sub-seasonal ECA from 1965–1976 to 2002–2013 is similar to the 1965–1976 minus 2002–2013 DJF-mean ECA difference (Fig. 1d) and whether such a change is mainly related to the interdecadal variation of the UB-NAO$^+$ events because most of the UB events are related to NAO$^+$ (Luo et al. 2016b). Our analysis reveals that there are 67 UB-NAO$^+$ (53%) events out of 126 UB events, but only 30 UB-NAO$^-$ (24%) events and 29 UB-NAO° (23%) events during 1950–2017. On average, UB-NAO$^+$ events (1.17 and 1.08 cases per winter) during 1965–1976 and 2002–2013 are more frequent than UB-NAO$^-$ events (0.67 and 0.42 cases per winter) and UB-NAO° events (0.58 and 0.22 cases per winter). Figure 4a–d show the time-mean horizontal fields of composite daily Z500 and SAT anomalies averaged over the blocking episode from lag − 10 to 10 days of UB and UB-NAO$^+$ events during 1950–2017 and their differences between 1965–1976 and 2002–2013. It is found that the spatial pattern of the UB-induced cold anomaly over Eurasia for UB-NAO$^+$ events (Fig. 4b) is similar to that for all UB events (Fig. 4a), although UB-NAO$^-$ and UB-NAO° events influence the cold anomalies over central Eurasia during 1965–1976 and 2002–2013 and have the same effect as UB-NAO$^+$ events (not shown). Because UB-NAO$^+$ events are much more frequent than UB-NAO$^-$ and UB-NAO° events, the decadal change of UB-induced sub-seasonal cold anomaly from 1965–1976 to 2002–2013 is mainly related to the decadal variation of UB-NAO$^+$ events. Over Eurasia, the difference of the UB-induced sub-seasonal cold anomaly between 1965–1976 and 2002–2013 (Fig. 4c) also resembles the DJF-mean SAT difference between the two periods (Fig. 2a), even though the strength of the cold anomaly is slightly different. Clearly, the 1965–1976 minus 2002–2013 sub-seasonal cold anomaly difference associated with UBs is mainly related to the change of UB-NAO$^+$ events from 1965–1976 to 2002–2013 (Fig. 4d) because the UB with NAO$^+$ (Fig. 4e, f) shows similar behaviors in persistence, movement and evolution to those of all UB events (Fig. 3e,

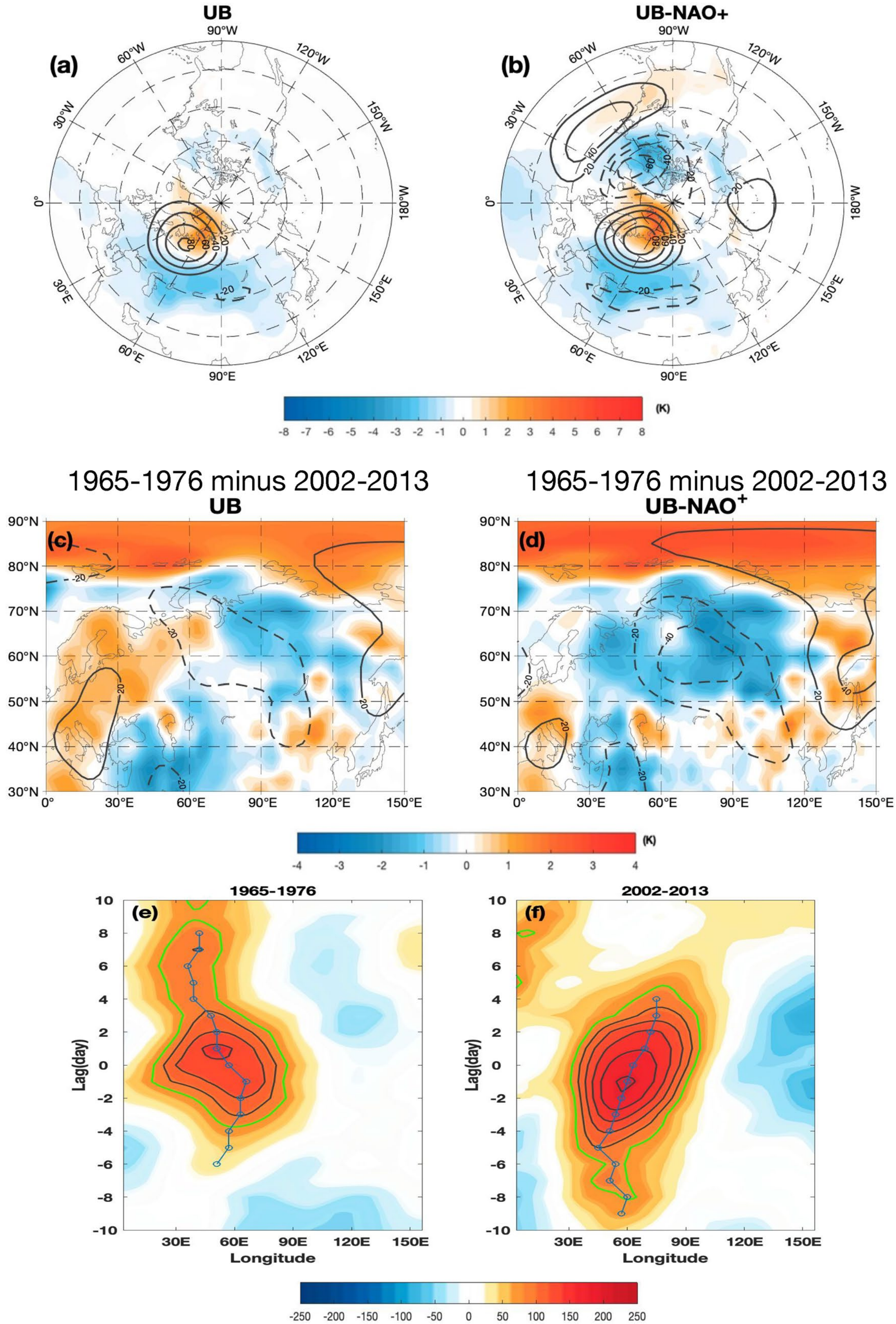
UB
UB-NAO+
(a)
(b)
(K)
1965-1976 minus 2002-2013
UB
UB-NAO+
(c)
(d)
(K)
1965-1976
2002-2013
(e)
(f)
Lag(day)
Longitude

◂**Fig. 4** Time-mean composite daily 500-hPa geopotential height (Z500) (contours, CI = 20 gpm) and SAT (color shading, unit: K) anomalies averaged from lag − 10 to 10 days (lag 0 denotes the peak day of blocking) for **a** UB and **b** UB-NAO$^+$ events during 1950–2017. **c**, **d** 1965–1976 minus 2002–2013 differences of time-mean Z500 and SAT anomalies for **c** UB and **d** UB-NAO$^+$ events, where the color shading represents the SAT anomaly region being significant at the 95% confidence level based on a two-sided Student t-test. **e**, **f** Time-longitude evolution of composite daily Z500 anomalies (unit: gpm and CI = 20 gpm) averaged over 50°–70° N of UB-NAO$^+$ events during **e** 1965–1976 and **f** 2002–2013. The 80 gpm contour is marked by the green line and the thick blue line with dot denotes the zonal location of the maximum daily Z500 anomaly and its temporal variation represents the movement speed

g). We also noted that the 1965–1976 minus 2002–2013 difference of the sub-seasonal cold anomaly associated with UBs is stronger in the upstream side of CE (especially to the south of 50° N) than in the downstream side of CE for UB or UB-NAO$^+$ events (Fig. 4c, d). Thus, in the following discussions we do not classify UB events according to the phase of NAO. Instead, we examine the modulation of AMO and IPO on UB and associated cold anomaly as well as their changes from 1965–1976 to 2002–2013, and the likely effect of the associated background conditions in Sects. 4–5.

4 Interdecadal variations of UB events and sub-seasonal ECA, and their linkage to IPO and AMO

4.1 Interdecadal SST modes and their linkages to IPO and AMO

Figure 5a, b show the normalized time series of the DJF-mean IPO and AMO indices during 1950–2017. In addition, we show the DJF-mean SST anomalies averaged over 1965–1976 and 2002–2013 in Fig. 5c, d, whereas the DJF-mean SST anomalies regressed onto the 9-year smoothed IPO and AMO indices are shown in Fig. 5e, f. It is shown that the winter IPO experienced a positive phase (IPO$^+$) during 1960–1968, 1979–1998 and 2015–2017; but a negative phase (IPO$^−$) during 1950–1959, 1970–1978 and 2000–2014 (Fig. 5a). The winter AMO had a positive phase (AMO$^+$) during 1950–1960 and 1996–2017; but a negative phase (AMO$^−$) during 1960–1995 (Fig. 5b). We find that there are 16 IPO$^−$ and 19 IPO$^+$ as well as 23 AMO$^−$ and 18 AMO$^+$ winters based on the 0.5 STD definition of the 9-year smoothed IPO and AMO indices during 1950–2017.

Clearly the SST anomaly patterns resemble those for IPO$^−$ and AMO$^−$ during 1965–1976 (Fig. 5c), but for IPO$^−$ and AMO$^+$ during 2002–2013 (Fig. 5d). The regressed SST anomalies show that while the IPO$^−$ mode corresponds to a weak AMO$^+$ SST anomaly over North Atlantic (Fig. 5e), the AMO$^+$ mode can correspond to an IPO$^−$ SST anomaly over the Pacific (Fig. 5f), whose amplitude is smaller than that of IPO$^−$ (Fig. 5e). Because the relationship between the IPO and AMO has been discussed in detail in other studies (e.g., Zhang and Delworth 2007; Meehl et al. 2021), examining their mutual relationship is not considered in our present study. A comparison of Fig. 5e, f with Fig. 5c, d leads us to infer that the 1965–1976 ECA is likely related to the IPO$^−$ and AMO$^−$ modes or their combination, whereas the 2002–2013 ECA is related to the IPO$^−$ and AMO$^+$ modes or their combination.

4.2 Modulation of IPO and AMO on UB and sub-seasonal cold anomalies

In this subsection, a composite of DJF-mean Z500 and SAT anomalies for two cases with and without UB events in IPO$^−$, AMO$^−$ and AMO$^+$ winters is first shown in Fig. 6 to help us consider whether IPO and AMO without UB contribute to the winter ECAs. Figure 6a shows that IPO$^−$ with UB corresponds to a strong winter cold anomaly over central Eurasia. However, when UB events are excluded from the IPO$^−$ winters, no strong cold anomaly appears over central Eurasia, but a weak cold anomaly can occur north of 60° N or to the east of 100° E for IPO$^−$ (Fig. 6b). For AMO$^+$ there is no strong ECA for both cases with and without UB (Fig. 6c, d). For AMO$^−$ a relatively strong cold anomaly is seen in the upstream and south sides of central Eurasia (Fig. 6e), but almost disappears when the UB events are excluded (Fig. 6f). Thus, AMO$^−$ without UB cannot produce interdecadal cold anomalies south of 60° N over Eurasia, but are linked to strong high-latitude cold anomalies over Eurasia (north of 60° N). Similar results are found using the zero threshold for defining the IPO and AMO phases (Fig. S6), even though the ECA is relatively weak. Thus, AMO$^+$ or AMO$^−$ cannot produce a strong cold anomaly over central Eurasia south of 60° N as seen in observations (Fig. 1b, c) if UB is absent. Similarly, IPO$^−$ without UB cannot contribute to the interdecadal cold anomalies over central Eurasia (Fig. 6b). These results, taken in concert, suggest that UB events modulated by IPO$^−$, AMO$^−$ and AMO$^+$ play a significant role in the winter cold anomaly over central Eurasia. By comparison, the interdecadal cold anomaly during IPO$^−$ without UB in the winter ECA contributes to a relatively weak cold anomaly in the downstream side of 100° E.

We show the time series of the event number of UB events in winter for IPO$^−$, IPO$^+$, AMO$^−$ and AMO$^+$ in Fig. 7. There are 36 (34) total UB events or 2.25 (1.79) UB events per winter during IPO$^−$ (IPO$^+$) (Fig. 7a, b), but 43 (33) total UB events or 1.87 (1.83) UB events per winter during ‘AMO$^−$ (AMO$^+$) (Fig. 7c, d). Thus, the UB event number does not vary greatly among the IPO$^−$, IPO$^+$, AMO$^−$ and AMO$^+$ phases. This is expected because UB (mostly UB-NAO$^+$) events are mainly excited by the decay

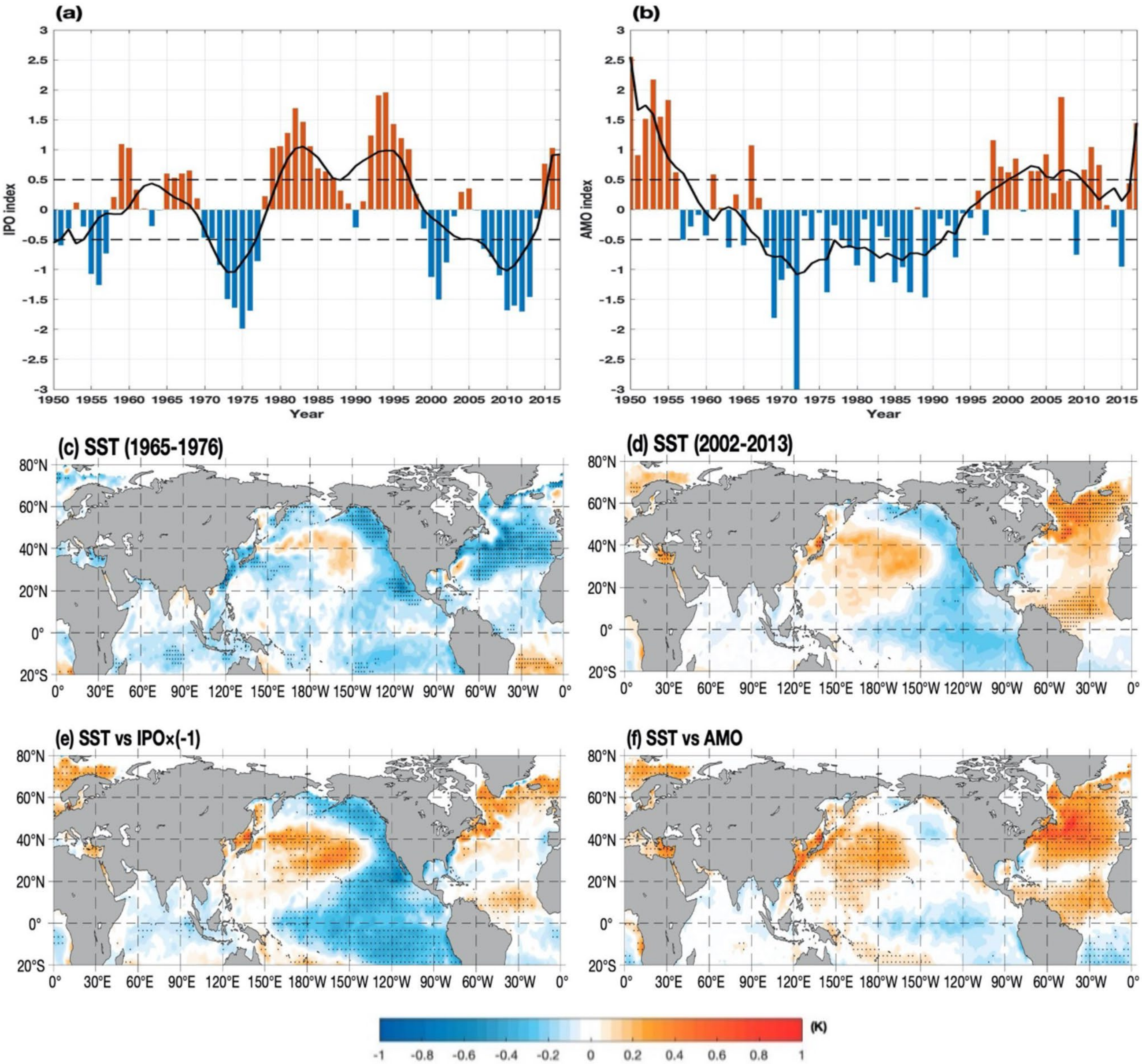

Fig. 5 **a**, **b** Time series of normalized DJF-mean **a** Interdecadal Pacific Oscillation (IPO) and **b** Atlantic Multidecadal Oscillation (AMO) indices during 1950–2017, where the black solid line represents a 9-year moving average. **c**, **d** Time-mean winter SST anomalies during **c** 1965–1976 and **d** 2002–2013. **e**, **f** regressed DJF-mean SST (color shading, in K per unit index) against the normalized **a** DJF-mean IPO index (multiplied by − 1.0) and **b** AMO index time series with a 9-year moving average. In panels **c**–**f**, the dot in the color shading represents the region being significant at the 95% confidence level based on a two-sided Student t-test

of NAO^+ via energy dispersion or the propagation of wave trains (Luo et al. 2016b), which does not strongly depend on the phase of IPO or AMO. However, IPO or AMO can modulate the interdecadal background condition and affect the longitudinal position, duration, movement and evolution of UB events.

To understand how the phase of IPO or AMO modulates the behaviors of UB and associated sub-seasonal ECA, it is useful to show the time-mean fields of composite daily Z500 and SAT anomalies averaged over a blocking period from lag − 10 to 10 days of UB events and time-longitude plots of the composite daily Z500 anomalies averaged over 50°–70° N in Figs. 8 and 9 for the two phases of IPO and AMO, respectively. It is seen that a strong sub-seasonal ECA appears over central Eurasia and its upstream side during the UB events for IPO^- (Fig. 8a) as UB has a strong positive height anomaly near 60° E and its west side, a long duration of about 9.5 days with rapid growth and persistent slow decay, and a small westward speed of about − 0.2 m/s in the Ural region mainly occurring after lag 3 (Fig. 8d). UB is mainly located in the west part of the Ural Mountains. In contrast, a weak ECA is seen for IPO^+ (Fig. 8b) as UB has a very weak positive Z500 anomaly, a shorter lifespan (~ 7 days), and a large retrogression speed of about − 2.0 m/s but without rapid growth and persistent slow decay (Fig. 8e). Thus, UB makes a larger contribution to the cold anomaly upstream of central Eurasia during IPO^- than during IPO^+ because of the westward displacement and long lifetime of UB and its rapid growth and slow decay during IPO^-.

A relatively intense cold anomaly is seen over central Eurasia and its upstream side during UB events for AMO^- (Fig. 9a) as UB has a positive height anomaly around 30°–60° E, a relatively short duration (~ 7 days), a westward movement of about − 1.0 m/s and a weaker slow decay for AMO^- (Fig. 9d) than for IPO^- (Fig. 8d). UB corresponds to a strong cold anomaly over central Eurasia and its downstream side for AMO^+ (Fig. 9b) because it shows slow growth and rapid decay with a duration of ~ 9 days and a large eastward speed of about 1.5 m/s (Fig. 9e). The UB duration difference of ~ 2 (3) days is significant at the 90% (95%) confidence level with for a Monte-Carlo test. These UB differences in longitudinal position, movement and duration lead to a large difference in the cold anomaly in the upstream and downstream sides of central Eurasia between AMO^+ and AMO^- (Fig. 9c). A comparison between Figs. 8 and 9 reveals that AMO^+ plays an important role in the UB-induced cold anomaly over CE and its downstream region (Fig. 9b) because of the long lifetime, eastward movement, slow growth and rapid decay of the composite UB. But the UB-induced sub-seasonal ECA is located more west- and south-ward during IPO^- than during AMO^+, although AMO^- contributes to the upstream cold anomaly through retrograding UBs with a slow decay.

4.3 Is the decadal change of the winter ECA due to decadal changes in UB-induced sub-seasonal ECAs modulated by IPO and AMO?

In this subsection, we quantitatively evaluate the contributions of UB events modulated by IPO^-, AMO^- and AMO^+ to the spatial changes of the winter SAT anomalies over CE. Because the 1965–1976 period includes both IPO^- and AMO^- winters and 2002–2013 corresponds to both IPO^- and AMO^+ winters, it is instructive to examine the change of the UB-induced sub-seasonal ECA from IPO^- or AMO^- in 1965–1976 to IPO^- or AMO^+ in 2002–2013. Based on this, one can understand whether the change of the winter ECA from 1965–1976 to 2002–2013 is mainly related to the interdecadal changes of UB-induced sub-seasonal ECAs modulated by IPO^-, AMO^- or AMO^+. It is seen from Fig. 7 that during 1965–1976 UB events occurred in the time period 1971–1976 (1968–1976) for IPO^- (AMO^-), but during 2002–2013 they occurred in the time period 2007–2013 (2002–2009) for IPO^- (AMO^+). This suggests that AMO^+ (IPO^-) mainly modulates the ECA via UB changes during the former (later) period of 2002–2013, while during 1965–1976 the winters of UB events associated with IPO^- are slightly different from those associated with AMO^-.

We show time-mean fields of the composite daily Z500 and SAT anomalies averaged from lag − 10 to 10 days of UB events in Fig. 10 for IPO^- and AMO^- during 1965–1976; and IPO^- and AMO^+ during 2002–2013 as well as the IPO^- (1965–1976) minus IPO^- (2002–2013) and AMO^- (1965–1976) minus AMO^+ (2002–2013) differences. It is found that for IPO^- the UB-induced sub-seasonal cold anomaly occurs mainly over central Eurasia and its upstream side (30°–70° E) during 1965–1976 (Fig. 10a), but over central Eurasia and its downstream side (90°–120° E) during 2002–2013 (Fig. 10b). This feature can be clearly seen from their difference field (Fig. 10c). During 1965–1976, the UB-induced Eurasian cold anomaly for AMO^- (Fig. 10d) has a similar spatial pattern to that for IPO^- (Fig. 10a), although they show a smaller difference. The UB-related cold anomaly for AMO^+ (Fig. 10e) is also similar to that for IPO^- during 2002–2013 (Fig. 10b), although the cold anomaly in the downstream region of CE is slightly stronger for IPO^- (Fig. 10b) than for AMO^+ (Fig. 10e). Thus, under the modulation of IPO^-, AMO^- and AMO^+ the UB-related sub-seasonal cold anomaly is stronger in the upstream side of CE during 1965–1976 than during 2002–2013. Based on UB events for the different phases of IPO and AMO (Fig. S7), similar results can be found from the composite of UB events (Fig. S8) if individual IPO and AMO phases are defined by using the zero threshold of the IPO and AMO indices, even though UB-related sub-seasonal ECA is the same for IPO^- and AMO^+ during 2002–2013.

Here, we further examine whether the change in the winter ECA from 1965–1976 to 2002–2013 is mainly related to the variation of UB events from IPO^- to AMO^+ during 1950–2017 or from IPO^- during 1965–1976 to AMO^+ during 2002–2013. We show the IPO^- (1965–1976) minus AMO^- (1965–1976), IPO^- (2002–2013) minus AMO^+ (2002–2013), IPO^- minus IPO^- (1965–1976), AMO^+ minus AMO^+ (2002–2013), IPO^- minus AMO^+, and IPO^- (1965–1976) minus AMO^+ (2002–2013) difference fields of time-mean Z500 and SAT anomalies averaged from lag − 10 to 10 days of UB events in Fig. 11. In this figure, the IPO^- (1950–2017) or AMO^+(1950–2017) is referred to as IPO^- or AMO^+. It is of interest to see that the UB-related sub-seasonal cold anomaly is slightly stronger in the upstream region of CE for IPO^- than for AMO^- during 1965–1976 (Fig. 11a), but stronger in the north of 50°N and in the downstream region of 100° E for IPO^- than AMO^+ during 2002–2013 (Fig. 11b). Such an effect becomes slightly weak during 1965–1976 when the phases of IPO

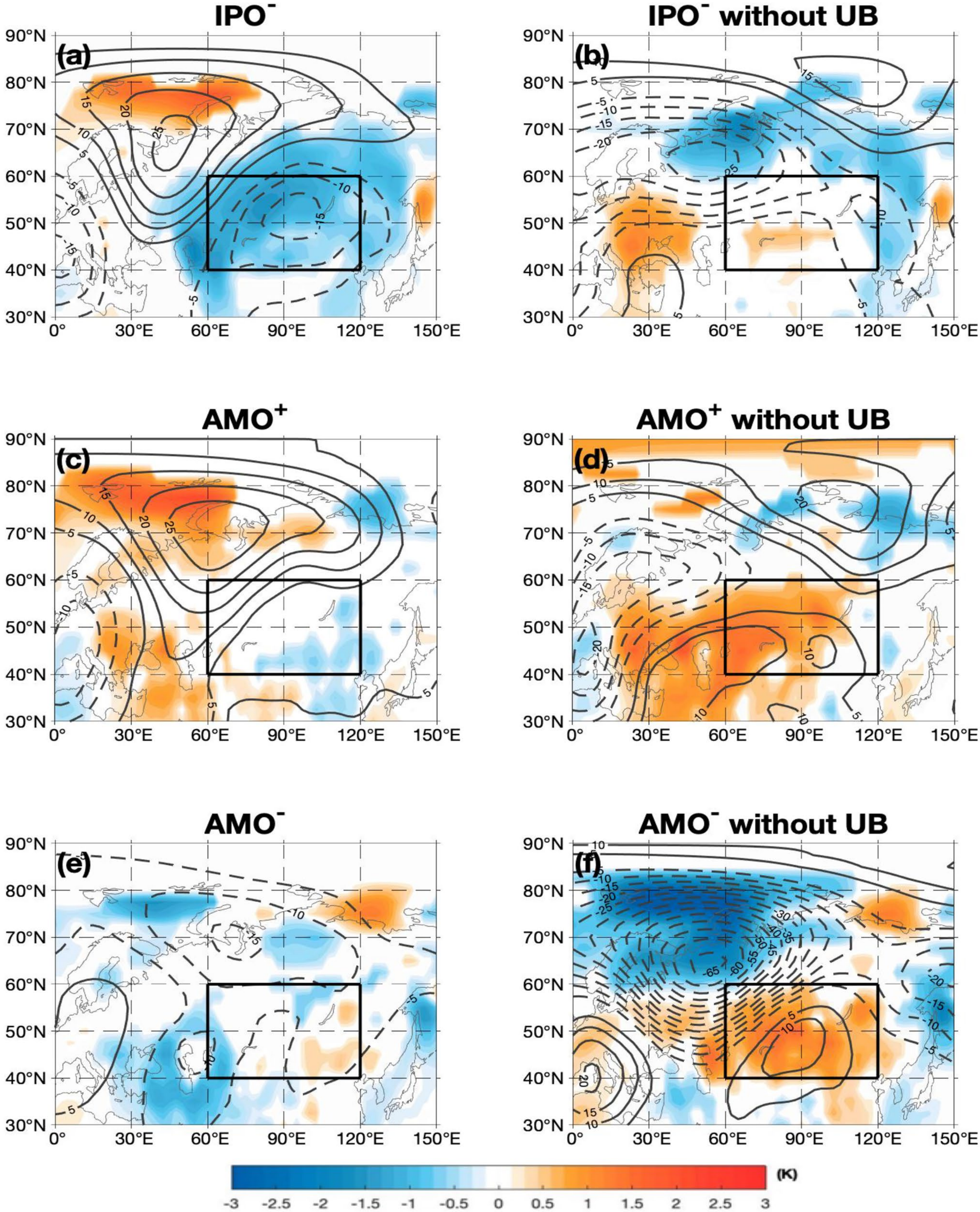

IPO⁻
(a)
IPO⁻ without UB
(b)
AMO⁺
(c)
AMO⁺ without UB
(d)
AMO⁻
(e)
AMO⁻ without UB
(f)
90°N
80°N
70°N
60°N
50°N
40°N
30°N
0°
30°E
60°E
90°E
120°E
150°E
(K)
-3
-2.5
-2
-1.5
-1
-0.5
0
0.5
1
1.5
2
2.5
3

◀**Fig. 6** Composite DJF-mean Z500 (contours, unit: gpm) and SAT (color shading) anomalies in **a**, **b** IPO^-, **c**, **d** AMO^+ and **e**, **f** AMO^- winters during 1950–2017 based on the 0.5 STD threshold value definition of 9-year smoothed IPO and AMO indices for days **a**, **c**, **e** with and **b**, **d**, **f** without UB events (the case without UB represents that blocking days from lag − 10 to 10 are removed for each UB event in winter). The composite field with UB events during IPO^- (AMO^- or AMO^+) is referred to as the IPO^- (AMO^- or AMO^+) case, whereas the composite field without UB events (blocking days from lag − 10 to 10 days are removed) during IPO^- (AMO^- or AMO^+) is referred to as the IPO^- (AMO^- or AMO^+) without UB case. Color shading represents the areas being significant at the 95% level based on a two-sided Student t-test. Black box represents central Eurasia or Siberia

and AMO are defined using the zero threshold (Fig. S9a), but the UB-related sub-seasonal cold anomaly has the same spatial pattern for IPO^- and AMO^+ during 2002–2013 (Fig. S9b). In brief, the IPO^- minus AMO^- SAT anomaly difference is small during 1965–1976, whereas the IPO^- minus AMO^+ difference during 2002–2013 is also small only in the south of 50° N.

It is also seen from Fig.11c, d that the UB-related sub-seasonal ECA is weaker for both IPO^- and AMO^+ during 1950–2017 than for IPO^- during 1965–1976 (Fig. 11c) or for AMO^+ during 2002–2013 (Fig. 11d). Over Eurasia the IPO^- minus AMO^+ SAT anomaly difference during 1950–2017 (Fig. 11e) has a spatial pattern similar to the IPO^- (1965–1976) minus AMO^+ (2002–2013) SAT anomaly difference (Fig. 11f), which also resembles the AMO^- (1965–1976) minus AMO^+ (2002–2013) difference (Fig. 10f). Thus, the decadal variation of UB-induced cold anomaly from 1965–1976 to 2002–2013 can be, to a large extent, explained by the change of the UB events associated with the transition from IPO^-/AMO^- during 1965–1976 to IPO^-/AMO^+ during 2002–2013.

To quantify changes in the UB-related sub-seasonal SAT anomaly from 1965–1976 to 2002–2013 in the upstream and downstream regions of CE, we show the time series of domain-averaged composite daily SAT anomalies over the upstream (30°–70° E, 30°–50° N) and downstream (90°–130° E, 30°–50° N) regions of UB events from lag − 20 to 20 days in Fig. 12a–f for IPO^-, AMO^- and AMO^+ during 1950–2017, 1965–1976 and 2002–2013. It is found that UBs associated with IPO^- and AMO^- during 1965–1976 contribute more significantly to sub-seasonal cold anomalies in the upstream region of CE than those associated with AMO^+ during 2002–2013 (Fig. 12e, f), even though the role of IPO^- (Fig. 12a) is more important than that of AMO^- (Fig. 12c). In contrast, UB events during AMO^+ contribute slightly more to the sub-seasonal cold anomaly in the downstream side of CE than during IPO^- and AMO^- (Fig. 12b, d, f). These results suggest that the decadal change of the winter ECA from 1965–1976 to 2002–2013 (Fig. 2a) is not only related to the interdecadal variations of the UB-induced sub-seasonal ECAs modulated by IPO^- and AMO^+, but also related to retrograde UBs during AMO^- winters.

Because 1965–1976 (2002–2013) includes IPO^- and AMO^- (IPO^- and AMO^+) as noted above, it is useful to further examine how the different IPO/AMO phase combinations modulate the UB and associated sub-seasonal ECA. Following the definition of the IPO and AMO phase combination in Sect. 2, we show winter UB events in Fig. 13a for the IPO^-/AMO^-, IPO^-/AMO^+, IPO^+/AMO^- and IPO^+/AMO^+ combinations. It is found that there are 10 IPO^-/AMO^-, 24 IPO^-/AMO^+, 22 IPO^+/AMO^- and 8 IPO^+/AMO^+ combination winters during 1950–2017, which correspond in turn to 25, 43, 42 and 16 UB events or 2.5, 1.79, 1.91 and 2 UB events per winter (Fig. 13a). We show time-mean fields of composite daily Z500 and SAT anomalies averaged from lag -10 to 10 days of UB events in Fig. 13b–g for these phase combinations. We can see that UB events are most frequent in the IPO^-/AMO^- winters and occurred during 1969–1978. In the IPO^-/AMO^+ winters UB events occurred during 1950–1959 and 2000–2014 (Fig. 13a). UB corresponds to strong sub-seasonal cold anomalies over CE for the IPO^-/AMO^- and IPO^-/AMO^+ combinations (Fig. 13b, c), although the UB-induced cold anomaly is stronger and located more southwest in the IPO^-/AMO^- combination (Fig. 13b) than in the IPO^-/AMO^+ combination (Fig. 13c). In contrast, the UB-induced cold anomalies are weak over central Eurasia for the IPO^+/AMO^- (Fig. 13e) and IPO^+/AMO^+ (Fig. 13f) combinations. It is also seen that the UB-induced cold anomaly for the IPO^-/AMO^- combination (Fig. 13b) has a spatial pattern similar to that for IPO^- (Fig. 10a) or AMO^- (Fig. 10d) in 1965–1976. In the IPO^-/AMO^+ combination winter, the UB-induced cold anomaly pattern (Fig. 13c) is analogous to that for the IPO^- (Fig. 10b) or AMO^+ (Fig. 10e) in 2002–2013. Moreover, it is found that the IPO^-/AMO^- minus IPO^-/AMO^+ difference of the UB-induced SAT anomaly (Fig. 13d) has a large similarity with the 1965–1976 minus 2002–2013 difference of the UB-induced SAT anomaly over CE (Fig. 4c). The IPO^-/AMO^- minus IPO^-/AMO^+ differences of the sub-seasonal SAT anomalies averaged over CE and its upstream region (30°–50° N, 30°–70° E) are 0.12 K and − 1.16 K, respectively, whereas the 1965–1976 minus 2002–2013 differences of the UB-induced SAT anomalies are 0.2 K and − 0.8 K, respectively. Clearly, the change in the UB-induced cold anomalies from 1965–1976 to 2002–2013 or from the IPO^-/AMO^- to IPO^-/AMO^+ is large in the upstream region of CE, but small over CE. Thus, the above results suggest that the decadal variation of the winter ECA from 1965–1976 to 2002–2013 is closely linked to the interdecadal changes of UB events modulated by IPO^-, AMO^- and AMO^+ during 1965–1976 and 2002–2013.

Fig. 7 **a**–**d** Time series of winter UB events during **a** IPO^{-}, **b** IPO^{+}, **c** AMO^{-} and **d** AMO^{+} based on the 0.5 STD thresholds of the normalized 9-year moving averaged IPO and AMO indices during 1950–2017. Note that the 2006 (1986) winter belongs to IPO^{-} or (IPO^{+}), which does not correspond to UB events

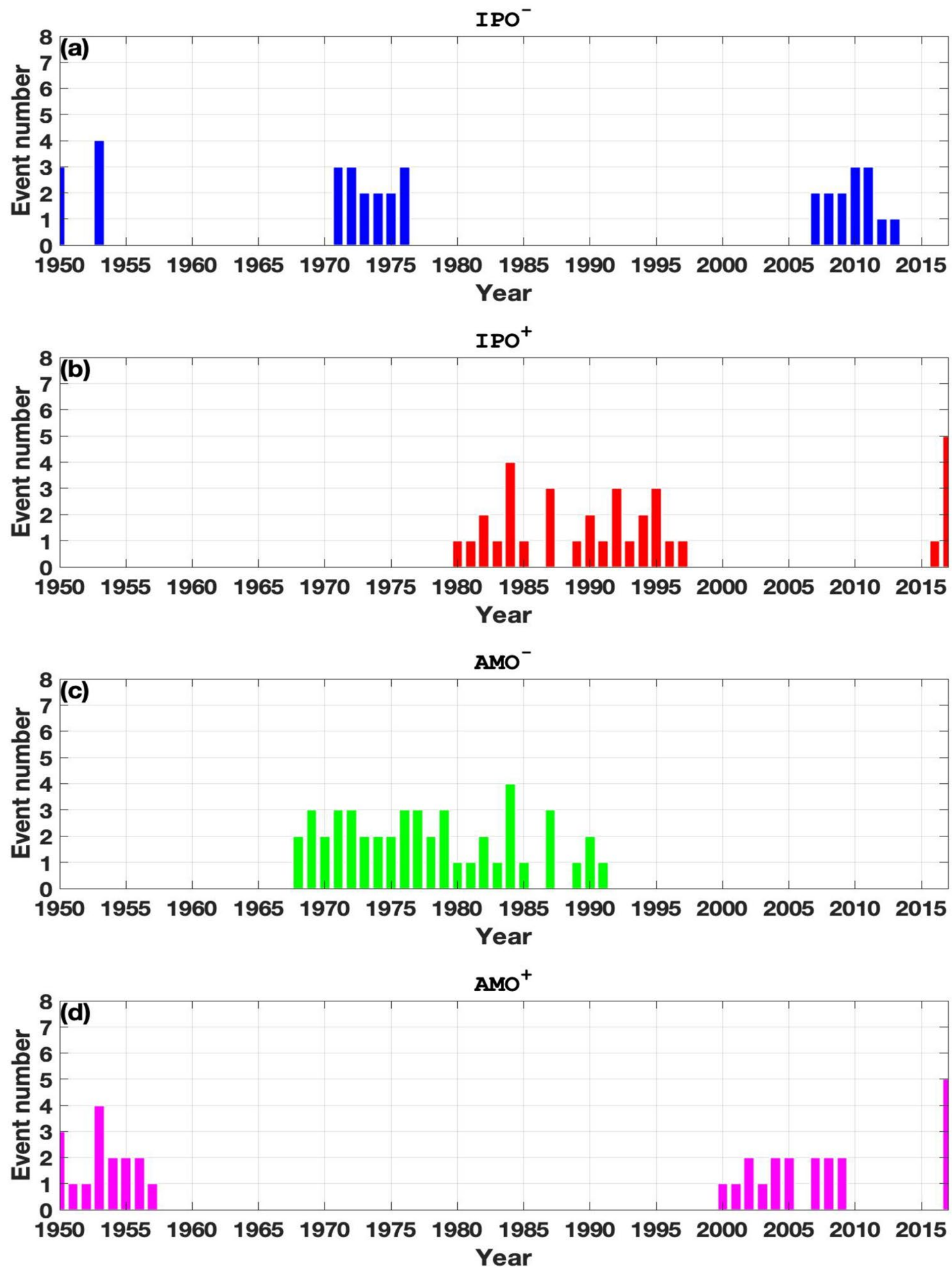

5 Atmospheric link between IPO/AMO and Ural blocking and ECA

In this section, we reveal why the phase of IPO or AMO can modulate UB and why a large SIC decline over BKS (Luo et al. 2019a; Simmonds and Li 2021) is unnecessary for the change of UB during IPO^{-}, which occurred during 1965–1976, but necessary for the UB change during AMO^{+}, which occurred during 2002–2013.

Figure 14 shows the regression patterns of DJF-mean U500, PV_y at 500 hPa and SIC anomalies against the 9-year smoothed DJF-mean IPO and AMO indices shown in Fig. 5a, b. One observes that during IPO^{-} there are negative U500 anomalies in the North Atlantic mid-high latitudes (42°–60° N) with a center near 50° N to the north of the Gulf Stream Extension (GSE) and over Eurasian high latitudes (north of 50° N) (Fig. 14a), as noted in Dong and Dai (2015). However, during AMO^{+} there are a positive U500 anomaly over the North Atlantic high latitudes (50°–65° N) centered near 60° N to the north of GSE and a negative U500 anomaly over the Ural Mountains and the east of 60° E (Fig. 14b). A reversed westerly wind pattern is seen for IPO^{+} or AMO^{-}.

Previous studies have indicated that the reduced winter zonal winds over North Atlantic mid-high latitudes (south of 60° N) and Eurasian high latitudes are related to the

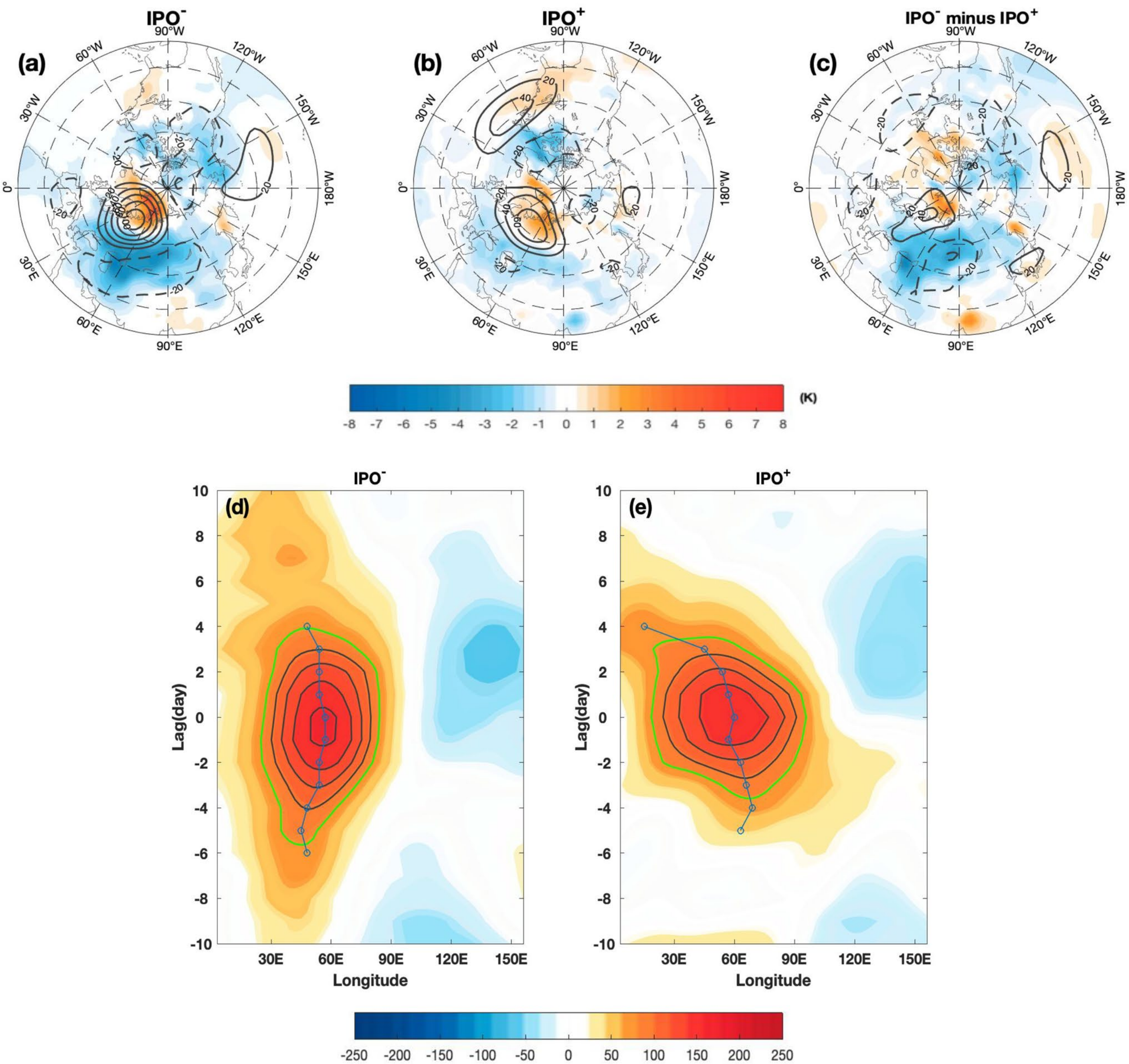

Fig. 8 Time-mean composite daily Z500 (contour; CI = 20 gpm) and SAT (color shading) anomalies averaged from lag −10 to 10 days (lag 0 denotes the peak day of blocking) of **a** 36 UB events during IPO$^-$ (16 cases), **b** 34 UB events during IPO$^+$ (19 cases) and **c** IPO$^-$ minus IPO$^+$ difference based on the 0.5 STD threshold of the 9-year moving averaged IPO index. **d**, **e** Time-longitude evolution of composite daily Z500 anomalies (contours; the green line represents 80 gpm and CI = 20 gpm) averaged over the latitudes 50°–70° N of UB events during **d** IPO$^-$ and **e** IPO$^+$. In panels **a**–**c**, the color shading represents the SAT anomaly region being significant at the 95% confidence level based on a two-sided Student t-test. In panels **d**–**e**, the thick blue line denotes the zonal location of the maximum daily Z500 anomaly and its temporal variation represents the movement speed

presence of a positive Z500 anomaly over the high latitudes (or a negative Arctic Oscillation) in winter. Such a positive Z500 anomaly is excited mainly by the weakened winter stratospheric polar vortex (Nakamura et al. 2016) occurring during the negative phase of Pacific Decadal Oscillation or IPO (Hu and Guan 2018). As a result, reduced westerly winds can occur over North Atlantic and Eurasian mid-high latitudes during IPO$^-$. However, the role of AMO$^+$ is to reduce the winter zonal winds in the Eurasian high latitudes through the intrusion of Atlantic warm waters into the BKS and BKS warming associated with the sea ice decline (Luo et al. 2017b). AMO$^+$ also enhances the winter zonal winds over North Atlantic (south of 60° N) via intensified meridional temperature gradients. Thus, in

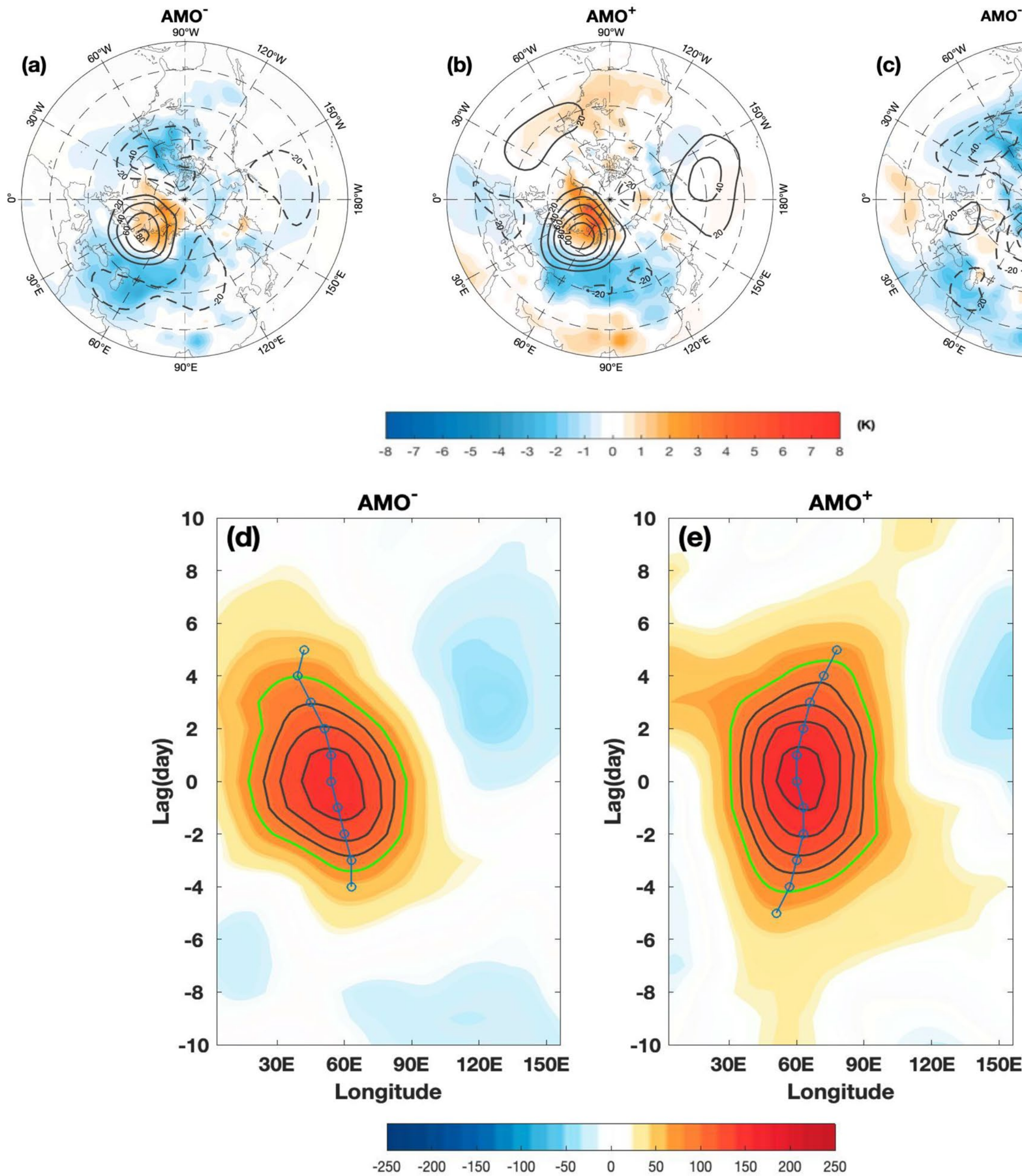

Fig. 9 Time-mean composite daily Z500 (contours, CI = 20 gpm) and SAT (color shading, in K) anomalies averaged from lag −10 to 10 days (lag 0 denotes the peak day of blocking) for the **a** 43 UB events during AMO$^-$ (23 cases), **b** 33 UB events during AMO$^+$ (18 cases) and **c** AMO$^-$ minus AMO$^+$ difference based on the 0.5 STD threshold of the 9-year moving averaged AMO index from 1950 to 2017. **d**, **e** Time-longitude evolution of composite daily Z500 anomalies (unit: gpm, the green line represents the 80 gpm contour and CI = 20 gpm) averaged over the latitudes 50°–70° N of the UB events during **d** AMO$^-$ and **e** AMO$^+$. In panels **a–c**, the color shading represents the region with SAT anomalies at the 95% confidence level based on a two-sided Student t-test. In panels **d–e**, the thick blue line denotes the zonal location of the maximum daily Z500 anomaly and its temporal variation represents the movement speed

this paper we did not further examine how IPO$^-$ and AMO$^+$ influence the background zonal winds over North Atlantic and Eurasia. While PV_y is weak (strong) in the mid-high latitude region 42°–57° N (50°–65° N) of the North Atlantic for IPO$^-$ (AMO$^+$), it is weak in Eurasian high latitudes near the Ural region (Fig. 14c, d). Moreover, we see that negative U500 and PV_y anomalies are insignificant over the North Atlantic for IPO$^-$ (Fig. 14a), whereas the negative U500 anomaly is insignificant over the Ural region for AMO$^+$ (Fig. 14b). However, a composite shows that the IPO$^-$ minus AMO$^+$ differences of the negative U500 and PV_y anomalies are significant over the North Atlantic and Ural region when the 0.5 STD threshold is used (Fig. S10). Thus, the North Atlantic zonal wind and PV_y patterns show

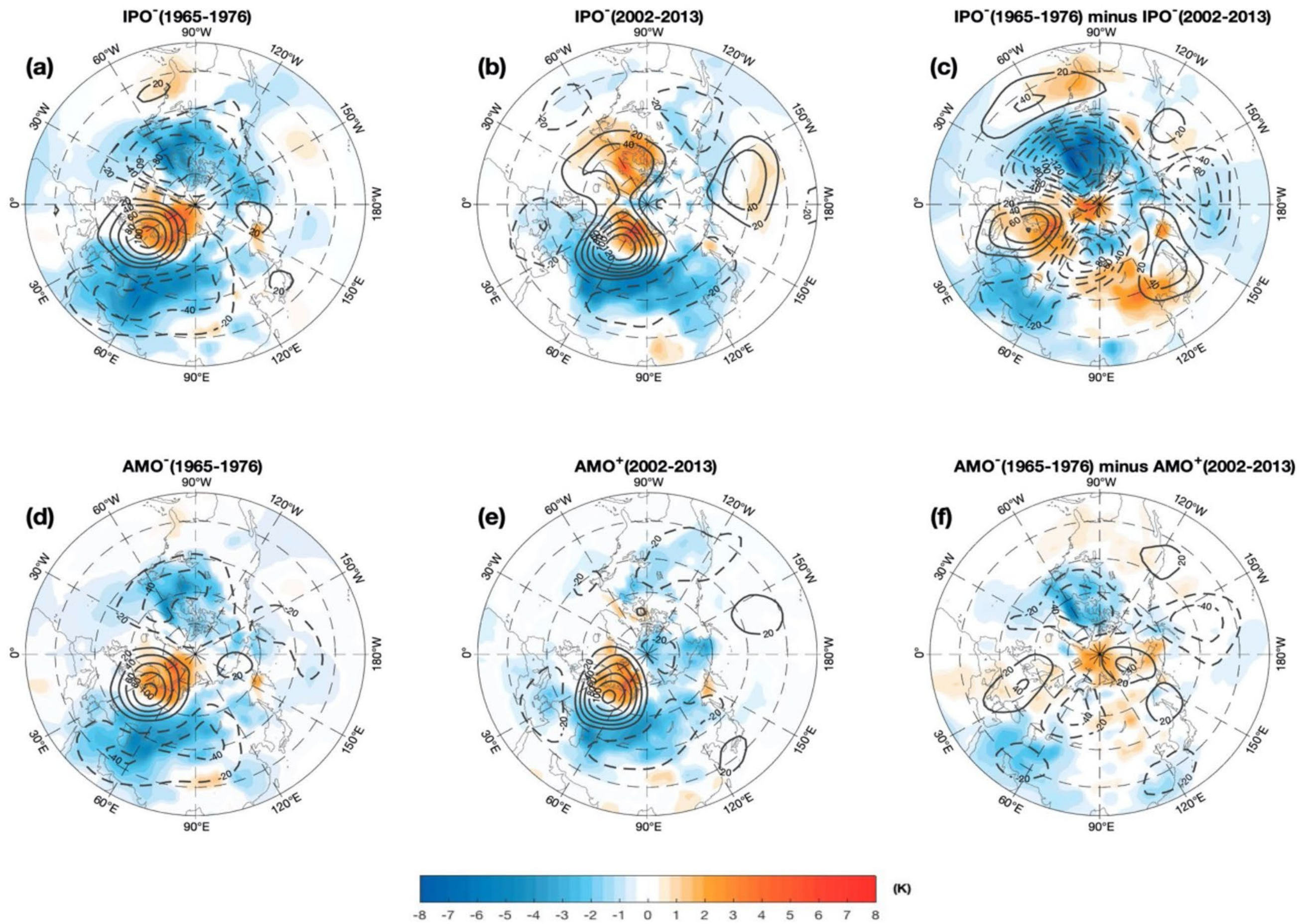

Fig. 10 Time-mean composite daily Z500 (contours, CI = 20 gpm) and SAT (color shading, in K) anomalies averaged from lag − 10 to 10 days (lag 0 denotes the peak day of blocking) of UB events for **a** IPO^- (15 UB events) and **d** AMO^- (22 UB events) during 1965–1976 and **b** IPO^- (14 UB events) and **e** AMO^+ (13 UB events) during 2002–2013 based on the 0.5 STD thresholds of 9-year smoothed IPO and AMO indices as well as the **c** IPO^- (1965–1976) minus IPO^- (2002–2013) and **f** AMO^- (1965–1976) minus AMO^+ (2002–2013) difference fields. The color shading represents the SAT anomaly region being significant at the 95% confidence level based on a two-sided Student t-test

significant changes between IPO^- and AMO^+, although they are weak in the Ural region.

In summary, weak zonal winds and small PV_y are seen in the mid-high latitude region from the south tip of Greenland to the Ural region and its east side for IPO^-. But for AMO^+ zonal winds and PV_y are strong in the south side of Greenland and weak in the Ural region. Based on the 9-year smoothed Z500 and SAT anomalies regressed onto the 9-year smoothed DJF-mean IPO and AMO indices (Fig. S11), it is noted that IPO^- corresponds to anticyclonic anomalies over Greenland and BKS (Fig. S11a), whereas AMO^+ corresponds to anticyclonic anomalies over the BKS and in the North Atlantic mid-high latitudes south of 60°N (Fig. S11b). The obtained 9-year smoothed Z500 and SAT anomalies can be approximately considered as the background circulation conditions of UB events. Thus, the interdecadal background conditions over the North Atlantic and Eurasia during 1965–1976 and 2002–2013 are significantly modulated by IPO^-, AMO^- and AMO^+.

According to the theoretical result of Zhang and Luo (2020), UB is long-lived, and shows rapid growth and slow decay when upstream background westerly winds and PV_y are weak as seen during IPO^-. In contrast, UB shows an enhanced eastward movement, slow growth and rapid decay when upstream background westerly winds and PV_y are relatively strong as seen during AMO^+. Thus, these results explain why UB shows an opposite change in movement and evolution between IPO^- and AMO^+ as seen in Figs. 8d and 9e. We also see that weak high-latitude westerly winds and small PV_y over Eurasia can occur without strong BKS warming or SIC decline for IPO^- (Luo et al. 2019a) because IPO^- corresponds to an interdecadal cold anomaly in Eurasian high latitudes (the north of 60° N) (Fig. S11a) with a decreased Arctic

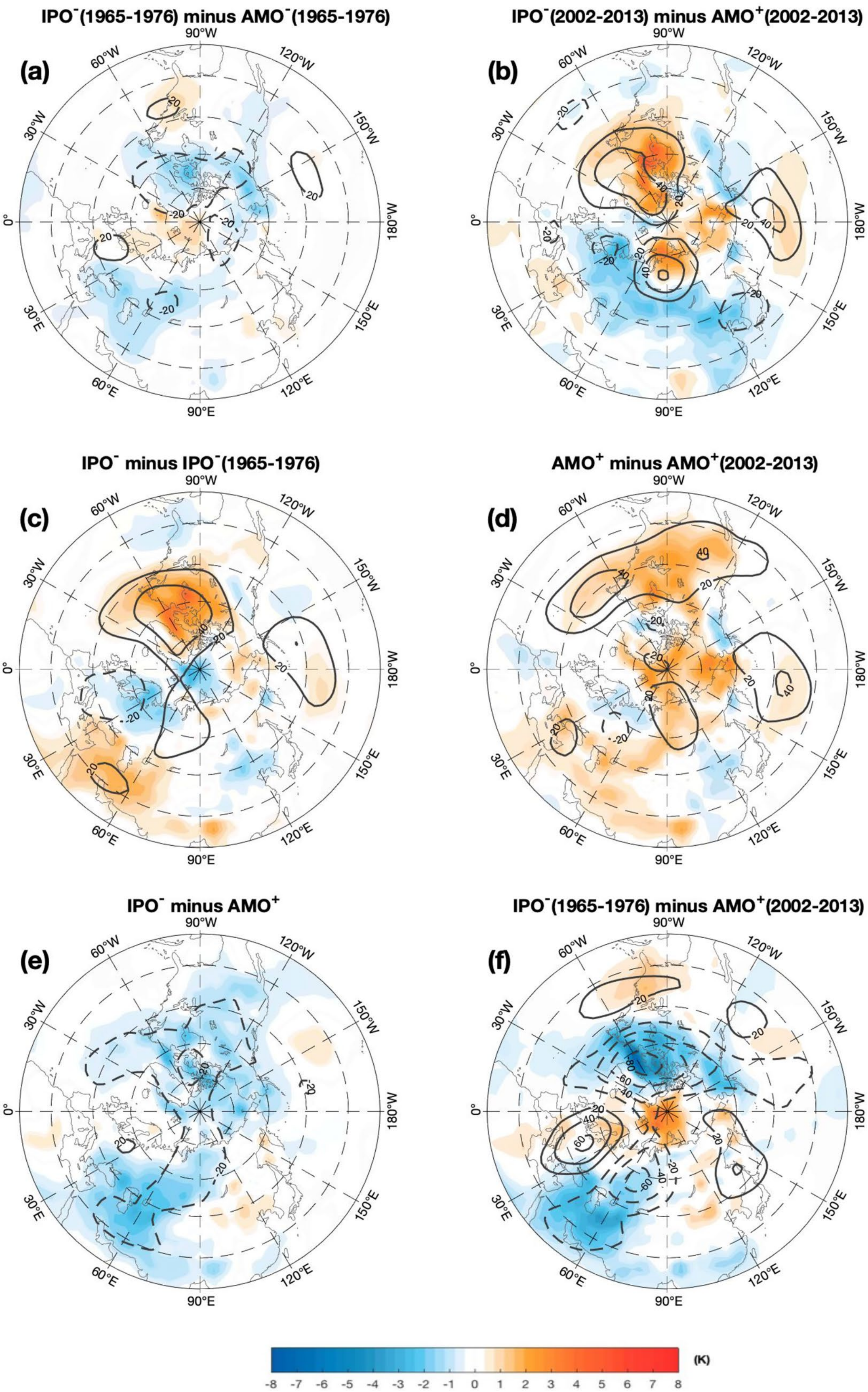
IPO⁻(1965-1976) minus AMO⁻(1965-1976)
(a)
IPO⁻(2002-2013) minus AMO⁺(2002-2013)
(b)
IPO⁻ minus IPO⁻(1965-1976)
(c)
AMO⁺ minus AMO⁺(2002-2013)
(d)
IPO⁻ minus AMO⁺
(e)
IPO⁻(1965-1976) minus AMO⁺(2002-2013)
(f)
90°W
60°W
120°W
30°W
150°W
0°
180°W
30°E
150°E
60°E
120°E
90°E
-8 -7 -6 -5 -4 -3 -2 -1 0 1 2 3 4 5 6 7 8
(K)

◂**Fig. 11** The difference fields of time-mean composite daily Z500 (contours, CI = 20 gpm) and SAT (color shading, in K) anomalies averaged from lag − 10 to 10 days (lag 0 denotes the peak day of blocking) of UB events for **a** IPO$^-$ (1965–1976) minus AMO$^-$ (1965–1976), **b** IPO$^-$ (2002–2013) minus AMO$^+$ (2002–2013), **c** IPO$^-$ minus IPO$^-$ (1965–1976), **d** AMO$^+$ minus AMO$^+$ (2002–2013), **e** IPO$^-$ minus AMO$^+$ and **f** IPO$^-$ (1965–1976) minus AMO$^+$ (2002–2013) based on the 0.5 STD thresholds of 9-year smoothed IPO and AMO indices. The IPO$^-$ or AMO$^+$ (1950–2017) is referred to as IPO- or AMO$^+$. The color shading represents the SAT anomaly difference region being significant at the 95% confidence level based on a two-sided Student t-test

high latitude PV anomaly and an increased Eurasian PV anomaly. Thus, the BKS SIC anomaly may be positive for IPO$^-$ (Fig. 14e), indicating that a low BKS SIC is not needed for the maintenance of UB for IPO$^-$ (Luo et al. 2019a), whereas AMO$^-$ has a similar effect. But a large BKS sea-ice loss is needed for increased persistence of UB for AMO$^+$ (Fig. 14f) because the AMO$^+$ in 2002–2013 needs a smaller PV anomaly over BKS and a small PV anomaly over Eurasia to maintain a small PV_y over Eurasia (Luo et al. 2019a). Such a small PV_y condition requires strong warming over BKS during 2002–2013 (Fig. S11b) in order to produce a stronger negative PV anomaly over BKS than to its south.

The above results explain why a strong winter ECA can occur during 1965–1976 even when IPO$^-$ or AMO$^-$ dominates and a large BKS SIC decline is absent (Fig. 14e). In contrast, the BKS warming and thus SIC decline must be strong for AMO$^+$ so that the winter ECA can occur during 2002–2013. Our finding here does not contradict the results of Mori et al. (2014), who showed a robust Eurasian cooling in the ensemble-mean response to recent Arctic sea-ice loss (but not in all individual realizations), because our result can not only explain why the BKS SIC decline must be strong for the ECA during 2002–2013, but also explain why the BKS SIC anomaly can be positive for the ECA during 1965–1976. Furthermore, greenhouse gas-induced warming and sea-ice loss are unlikely to cause cooling over Eurasia (Dai and Song 2020); thus, the ECA more likely results from internal decadal variations of UB associated with internal modes such as the IPO, AMO and Arctic decadal variations.

The above results reveal that AMO$^+$ favors eastward-moving, slowly growing and rapidly decaying UBs over Eurasia through intensified (weakened) high-latitude zonal winds and PV_y over the North Atlantic (Eurasia), whereas IPO$^-$ promotes the slow westward- moving, rapidly growing and slowly decaying UBs through weakened high-latitude zonal winds and PV_y from the North Atlantic toward Eurasia. But UBs are relatively short-lived and rapidly retrograde during AMO$^-$ and IPO$^+$ because the zonal winds and PV_y conditions are opposite to those during AMO$^+$ and IPO$^-$.

6 Summary and conclusions

In this paper, we first examined the dependence of winter Ural blocking (UB) and its impact on Eurasian surface air temperature (SAT) on the phase of IPO and AMO as defined by 9-year smoothed IPO and AMO indices, and then combined the recent IPO and AMO phases to physically explain the decadal difference in the winter Eurasian cold anomaly (ECA) between 1965–1976 and 2002–2013. A strong winter ECA is found to occur more in the upstream and southwestern side of central Eurasia during 1965–1976 than during 2002–2013. Although UB is not a necessary condition for winter ECA (Kim et al. 2021), the presence of UB can significantly strengthen winter ECA or the warm Arctic-cold Eurasia pattern (Luo et al. 2016a). This decadal change of the winter SAT anomaly from 1965–1976 to 2002–2013 is found to be mainly related to IPO$^-$, AMO$^-$ and AMO$^+$ through the modulation of the movement, persistence and evolution of Ural blocking (UB), rather than its event frequency (event numbers). In contrast, without UB the impact of IPO$^-$ and AMO$^-$ on the cold SAT anomaly is mainly confined to the north of 60° N over Eurasia or in part the east of 100° E. We propose a new pathway of the IPO/AMO–ECA connection, which works by means of the UB change due to the changed background condition related to the phase of the IPO or AMO: different IPO/AMO phases lead to different background westerly winds and PV_y over the North Atlantic and Eurasia, which affect the characteristics of UB, which in turn affect SAT over Eurasia through cold advection.

The 1965–1976 period was dominated by a negative phase IPO (IPO$^-$) in combination with a negative phase AMO (AMO$^-$), while a positive phase AMO (AMO$^+$) in combination with IPO$^-$ are frequent during 2002–2013. Although the event frequency of winter UB events does not strongly depend on the phase of IPO or AMO during 1950–2017, we found that UB is long-lived and shows weak retrogression, rapid growth and slow decay (eastward movement, slow growth and rapid decay) during IPO$^-$ (AMO$^+$), but is relatively short-lived and rapidly retrograde during both IPO$^+$ and AMO$^-$. During IPO$^-$ UB leads to a strong cold anomaly with a southwestward extension of central Eurasia through advection of cold Arctic air into these regions. AMO$^-$ has a similar effect because UB shows a retrogression, even though UB is relatively short-lived compared to that during IPO$^-$. During AMO$^+$ UB induces strong cold anomalies over central Eurasia or its downstream side through advection of cold Arctic air. It is found that the change of the winter ECA from 1965–1976 to 2002–2013 is mainly related to the different modulations of IPO$^-$, AMO$^-$ and AMO$^+$

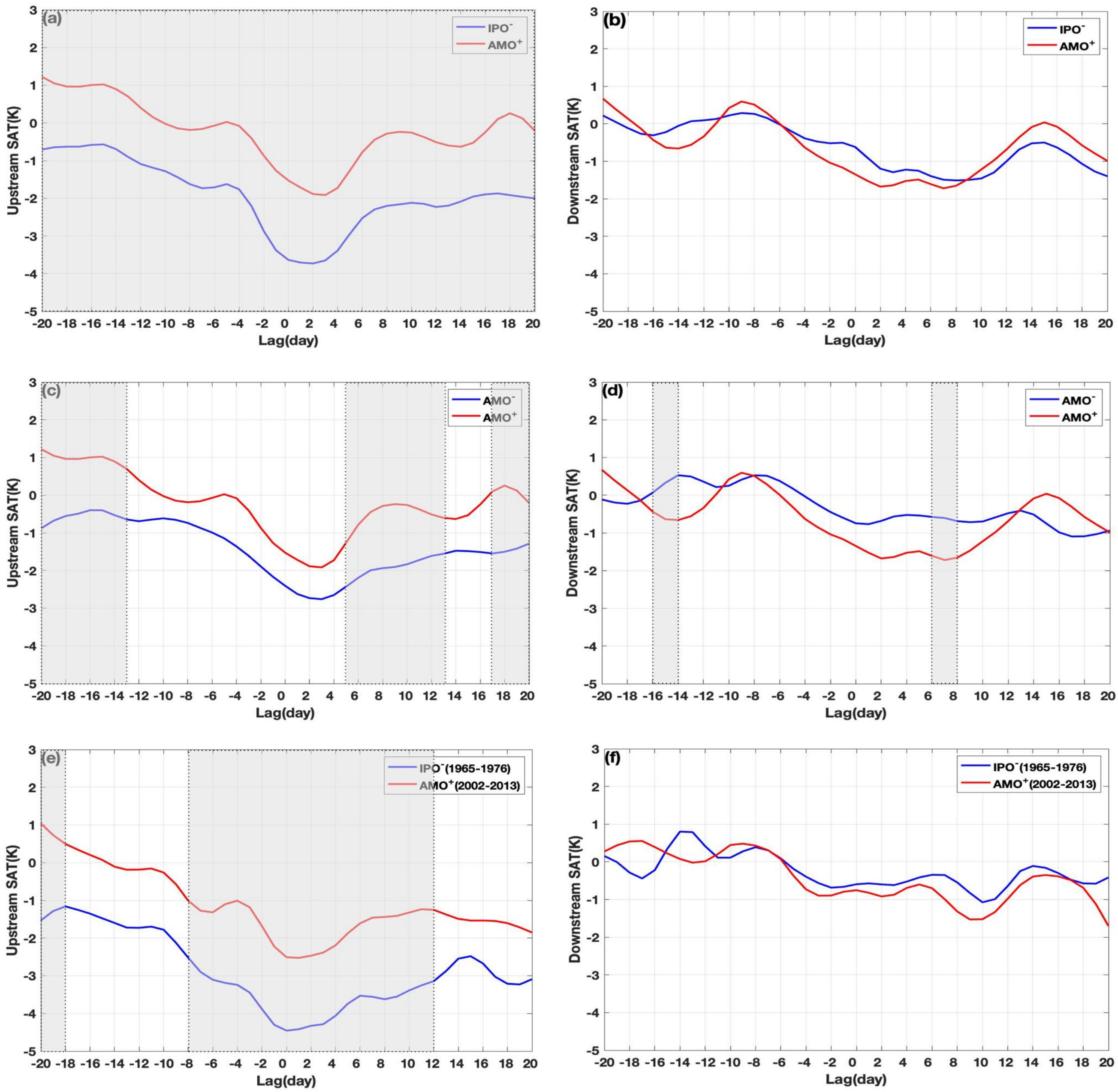

Fig. 12 Time evolution of composite daily SAT anomalies averaged over **a**, **c**, **e** upstream (30°–50° N, 30°–70° E) and **b**, **d**, **f** downstream (30°–50° N, 90°–130° E) regions, referred to as upstream and downstream SAT anomalies, during the UB life cycle from lag −20 to 20 days (lag 0 denotes the peak day) for UB events during IPO$^-$ (blue line), AMO$^-$ (blue line) and AMO$^+$ (red line) during **a–d** 1950–2017 and **e**, **f** 1965–1976 and 2002–2013 based on the 0.5 STD thresholds of 9-year smoothed IPO and AMO indices. The gray shading represents the difference of two curves being significant at the 95% confidence level for a Monte-Carlo test based on a 5000 times simulation

on the longitudinal position, persistence, movement and evolution of UB. To some extent, the difference of the UB-induced sub-seasonal cold anomaly between the IPO$^-$/AMO$^-$ to IPO$^-$/AMO$^+$ combinations can explain the change of the UB-related sub-seasonal ECA from 1965–1976 to 2002–2013.

We have also found that during IPO$^-$ without UB the background zonal winds and meridional PV gradient (PV_y) over Eurasian high latitudes are weakened due to reduced meridional temperature gradients and intensified PV anomalies related to strong background cold anomaly in the high-latitude Eurasia without strong warming or SIC decline over Barents–Kara Seas (BKS). Such zonal wind and PV_y changes over Eurasian high latitudes favor long-lived UBs, which are also seen during AMO$^+$ and related to an intense warming or SIC decline in BKS because the

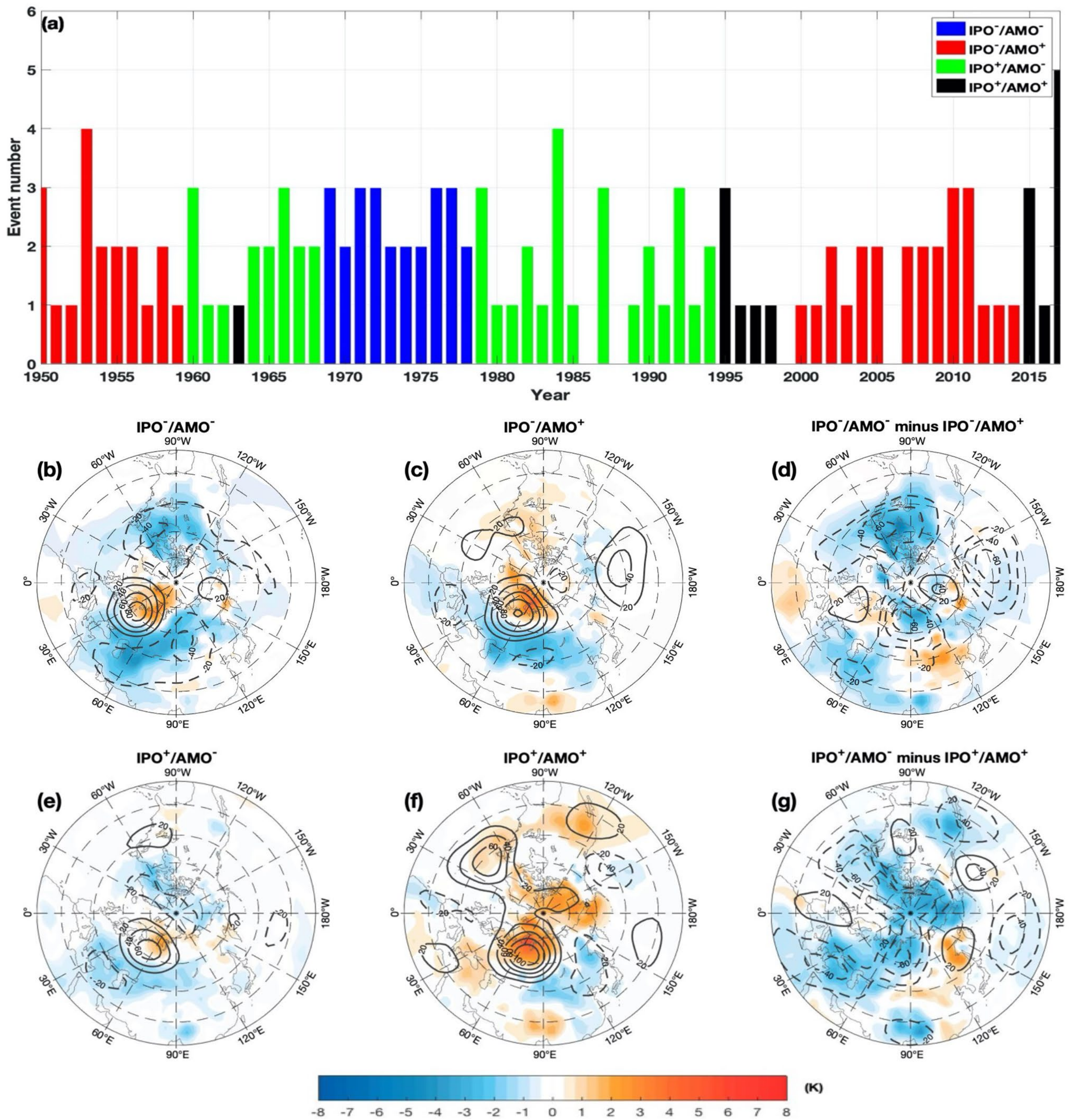

Fig. 13 **a** Time series of UB events in winter for IPO$^-$ /AMO$^-$ (10 cases, blue), IPO$^-$/AMO$^+$ (24 cases, red), IPO$^+$/AMO$^-$ (22 cases, green), and IPO$^+$/AMO$^+$ (8 cases, black) combinations based on the zero thresholds of 9-year smoothed IPO and AMO indices. **b**–**g** Time-mean Z500 (contour, CI = 20 gpm) and SAT (color shading) anomalies averaged from lag − 10 to 10 days (lag 0 denotes the peak day of blocking) of 25, 43, 42 and 16 UB events during **b** IPO$^-$/AMO$^-$, **c** IPO$^-$/AMO$^+$, **e** IPO$^+$/AMO$^-$, and **f** IPO$^+$/AMO$^+$ combinations as well as **d** IPO$^-$/AMO$^-$ minus IPO$^-$/AMO$^+$ and **g** IPO$^+$/AMO$^-$ minus IPO$^+$/AMO$^+$ differences. In panels **b**–**g**, the color shading represents the region being significant at the 95% confidence level based on a two-sided Student t-test

background warm anomaly prevails over Eurasian mid-high latitudes (Fig. S11b). During IPO$^-$ (AMO$^+$) weakened (intensified) westerly winds are also seen over the North Atlantic high latitudes (Fig. 14a, b) because of the presence of weak positive Z500 anomalies over the North Atlantic to the north (south) of 60° N (Fig. S10), which lead to the rapid growth, slow decay and retrogression (slow growth, rapid decay and eastward movement) of UB

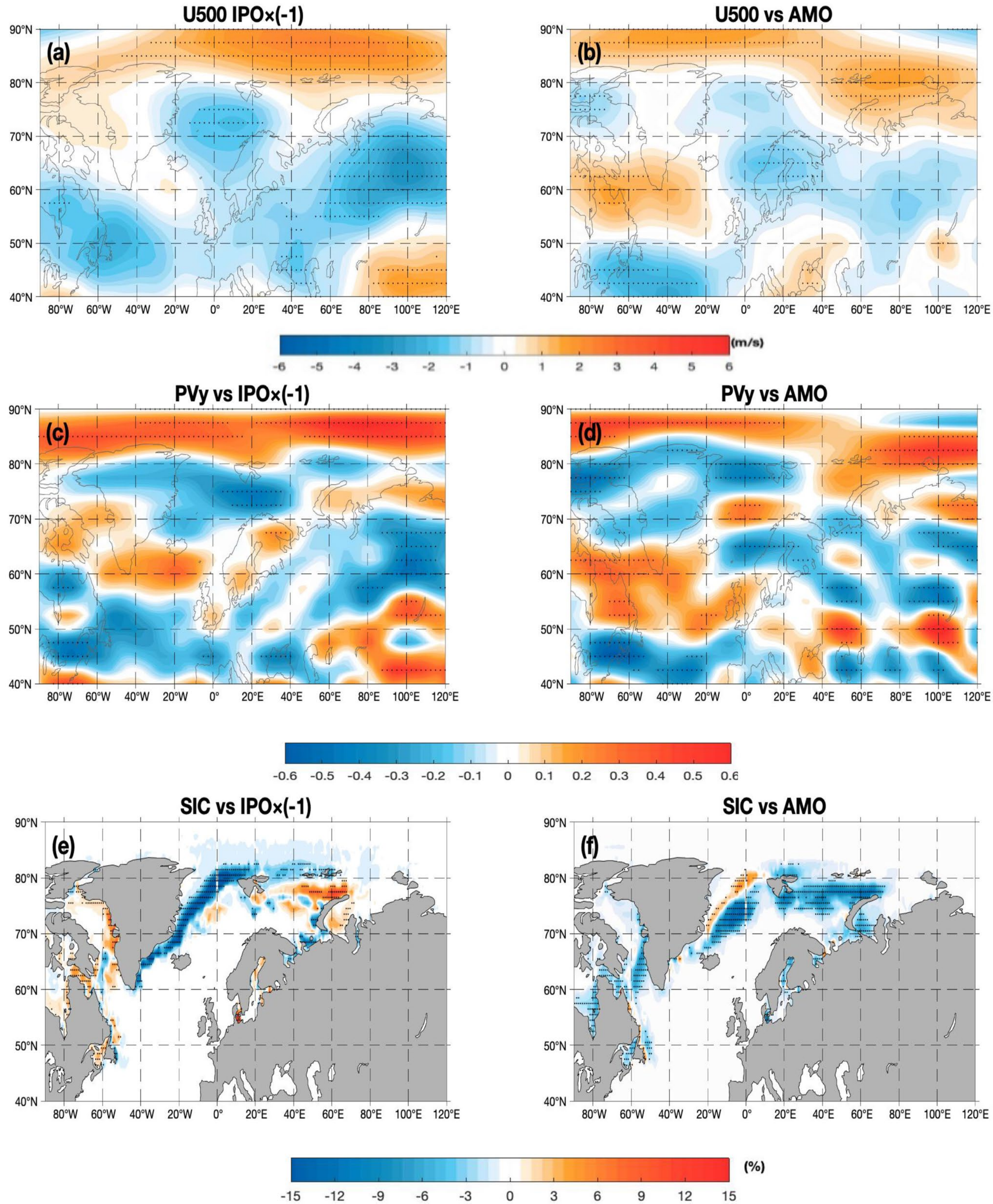

Fig. 14 DJF-mean **a**, **b** U500, **c**, **d** non-dimensional PVy for UB events removed and **e**, **f** DJF-mean SIC anomalies without UB events regressed onto the time series of normalized 9-year smoothed DJF-mean **a**, **c**, **e** IPO index (multiplied by −1.0) and **b**, **d**, **f** AMO index. The dot represents the color shading region being significant at the 95% confidence level for a two-sided Student t-test

mainly during its decaying phase for IPO$^-$ (AMO$^+$). The reversed zonal wind patterns are seen for IPO$^+$ (AMO$^-$).

In summary, our main results are that the large difference in UB's position, movement and evolution between IPO$^-$, AMO$^-$ and AMO$^+$ is important for the decadal variation of the winter ECA from 1965–1976 to 2002–2013. A strong BKS warming (or SIC decline) is necessary for a strong winter ECA for AMO$^+$, but is not necessary for IPO$^-$. Rudeva and Simmonds (2021) have also pointed to the role of the high-latitude background wind field in permitting or denying the establishment of quasi-stationary teleconnection patterns. Specifically, IPO$^-$ influences the ECA via the following pathway: IPO$^-$→ weak westerly winds and small PV_y over Eurasian high latitudes and North Atlantic mid-high latitudes → long-lived and westward-shifted UB with rapid growth and slow decay → upstream ECA. In contrast, AMO$^+$ influences the ECA via the following pathway: AMO$^+$→ weak westerly winds and small PV_y over Eurasian high latitudes as well as strong zonal winds and large PV_y over North Atlantic high latitudes (different from those over the North Atlantic for IPO$^-$)→ long-lived UB with eastward movement, slow growth and rapid decay → ECA over CE or its downstream side. Thus, the role of AMO$^+$ is to cause long-lived UB with eastward movement, slow growth and rapid decay and ECA over CE or its downstream side through enhancing upstream zonal winds and PV_y, whereas the role of IPO$^-$ is to cause long-lived UB occurring in the upstream side of the Ural region with rapid growth and slow decay and ECA over CE and its upstream side through reduced upstream zonal winds and PV_y. These different roles of IPO$^-$, AMO$^-$ and AMO$^+$ in the longitudinal position, movement and evolution of the UB and ECA and in the change of the winter ECA from 1965–1976 to 2002–2013 are not revealed in previous studies (e.g., Luo et al. 2017b; Sung et al. 2018; Luo et al. 2019a, b, c; Chen et al. 2021).

Although the NECP reanalysis data from 1950 to 2017 used in this paper is relatively short for sampling the IPO or AMO, the obtained results are likely reliable because the used data include one cycle of the AMO and at least one cycle for the IPO. Our future studies will use other long-term reanalysis datasets, as well as carefully-designed numerical model experiments directed at exploring the mechanisms highlighted here.

Supplementary Information The online version contains supplementary material available at https://doi.org/10.1007/s00382-021-06119-7.

Acknowledgements The idea of this manuscript was began in 2018 and finished in 2020. This research was supported by the Chinese Academy of Sciences Strategic Priority Research Program (Grant XDA19070403) and the National Natural Science Foundation of China (Grant numbers: 41790473 and 41975068). A. Dai acknowledges the funding support from the U.S. National Science Foundation (Grant nos. AGS-2015780 and OISE-1743738).

References

Booth BBB, Dunstone NJ, Halloran PR, Andrews T, Bellouin N (2012) Aerosols implicated as a prime driver of twentieth-century North Atlantic climate variability. Nature 484:228–232. https://doi.org/10.1038/nature10946

Chen Y, Luo D, Zhong L (2021) North Atlantic multidecadal footprint of the recent winter warm Arctic–cold Siberia pattern. Clim Dyn 57:121–139. https://doi.org/10.1007/s00382-021-05698-9

Cohen J et al (2014) Recent Arctic amplification and extreme mid-latitude weather. Nat Geosci 7:627–637. https://doi.org/10.1038/ngeo2234

Dai A (2013) The influence of the inter-decadal Pacific oscillation on US precipitation during 1923–2010. Clim Dyn 41:633–646. https://doi.org/10.1007/s00382-012-1446-5

Dai A, Song M (2020) Little influence of Arctic amplification on midlatitude climate. Nat Clim Chang 10:231–237. https://doi.org/10.1038/s41558-020-0694-3

Dai X, Wang P (2018) Identifying the early 2000s hiatus associated with internal climate variability. Sci Rep 8:13602. https://doi.org/10.1038/s41598-018-31862-z

Dai A, Fyfe JC, Xie S-P, Dai X (2015) Decadal modulation of global surface temperature by internal climate variability. Nat Clim Change 5:555–559. https://doi.org/10.1038/nclimate2605

Deser C, Guo R, Lehner F (2017) The relative contributions of tropical Pacific sea surface temperatures and atmospheric internal variability to the recent global warming hiatus. Geophys Res Lett 44:7945–7954. https://doi.org/10.1002/2017GL074273

Diao Y, Li J, Luo D (2006) A new blocking index and its application: blocking action in the Northern Hemisphere. J Clim 19:4819–4839

Dong B, Dai A (2015) The influence of the Interdecadal Pacific Oscillation on Temperature and Precipitation over the Globe. Clim Dyn 45:2667. https://doi.org/10.1007/s00382-015-2500-x

Dong B, Dai A, Vuille M, Elison Timm O (2018) Asymmetric modulation of ENSO teleconnections by the Interdecadal Pacific Oscillation. J Clim 31:7337–7361. https://doi.org/10.1175/JCLI-D-17-0663.1

Hersbach H et al (2020) The ERA5 global reanalysis. Q J R Meteorol Soc 146:1999–2049. https://doi.org/10.1002/qj.3803

Hu D, Guan C (2018) Decadal relationship between the stratospheric Arctic vortex and Pacific Decadal Oscillation. J Clim 31:3371–3386

Hua W, Dai A, Qin M (2018) Contributions of internal variability and external forcing to the recent Pacific decadal variations. Geophys Res Lett 45:7084–7092. https://doi.org/10.1029/2018GL079033

Huang JP, Xie YK, Guan XD, Li DD, Ji F (2017) The dynamics of the warming hiatus over the northern hemisphere. Clim Dyn 48:429–446. https://doi.org/10.1007/s00382-016-3085-8

Huang D, Dai A, Yang B (2019) Contributions of different combinations of the IPO and AMO to recent changes in winter East Asian jets. J Clim 32:1607–1625

Jin C, Wang B, Yang Y-M, Liu J (2020) "Warm Arctic-cold Siberia" as an internal mode instigated by North Atlantic warming. Geophys Res Lett 47:e2019GL086248. https://doi.org/10.1029/2019GL086248

Kalnay E et al (1996) The NCEP/NCAR 40-Year Reanalysis project. Bull Am Meteorol Soc 77:437–471. https://doi.org/10.1175/1520-0477(1996)077,0437:TNYRP.2.0.CO;2

Kaplan A, Cane MA, Kushnir Y, Clement AC, Blumenthal MB, Rajagopalan B (1998) Analyses of global sea surface temperature 1856–1991. J Geophys Res 103:18567–18589. https://doi.org/10.1029/97JC01736

Kim H-J, Son S-W, Moon W, Kug J-S, Hwang J (2021) Subseasonal relationship between Arctic and Eurasian surface air temperature. Sci Rep 11:4081. https://doi.org/10.1038/s41598-021-83486-5

Li C, Stevens B, Marotzke J (2015) Eurasian winter cooling in the warming hiatus of 1998–2012. Geophys Res Lett 42:8131–8139. https://doi.org/10.1002/2015GL065327

Li M, Luo D, Simmonds I, Dai A, Zhong L, Yao Y (2021) Anchoring of atmospheric teleconnection patterns by Arctic Sea ice loss and its link to winter cold anomalies in East Asia. Int J Climatol 41:547–558. https://doi.org/10.1002/joc.6637

Luo D, Xiao Y, Yao Y, Dai A, Simmonds I, Franzke CLE (2016a) Impact of Ural blocking on winter warm Arctic–cold Eurasian anomalies. Part I: blocking induced amplification. J Clim 29:3925–3947. https://doi.org/10.1175/JCLI-D-15-0611.1

Luo D, Xiao Y, Diao Y, Dai A, Franzke CLE, Simmonds I (2016b) Impact of Ural Blocking on winter Warm Arctic-Cold Eurasian anomalies. Part II: the link to the North Atlantic Oscillation. J Climate 29:3949–3971. https://doi.org/10.1175/JCLI-D-15-0612.1

Luo B, Luo D, Wu L, Zhong L, Simmonds I (2017a) Atmospheric circulation patterns which promote winter Arctic sea ice decline. Environ Res Lett 12:054017. https://doi.org/10.1088/1748-9326/aa69d0

Luo D, Chen Y, Dai A, Mu M, Zhang R, Simmonds I (2017b) Winter Eurasian cooling linked with the Atlantic Multidecadal Oscillation. Environ Res Lett 12:125002

Luo D, Chen X, Dai A, Simmonds I (2018) Changes in atmospheric blocking circulations linked with winter Artic warming: a new perspective. J Clim 31:7661–7677

Luo B, Wu L, Luo D, Dai A, Simmonds I (2019a) The winter midlatitude-Arctic interaction: effects of North Atlantic SST and high-latitude blocking on Arctic sea ice and Eurasian cooling. Clim Dyn 52(5–6):2981–3004. https://doi.org/10.1007/s00382-018-4301-5

Luo D, Chen X, Overland J, Simmonds I, Wu Y, Zhang P (2019b) Weakened potential vorticity barrier linked to recent winter Arctic sea ice loss and midlatitude cold extremes. J Clim 32:4235–4261

Luo D, Zhang W, Zhong L, Dai A (2019c) A nonlinear theory of atmospheric blocking: a potential vorticity gradient view. J Atmos Sci 76:2399–2427

Luo B, Luo D, Dai A, Simmonds I, Wu L (2021) A connection of winter Eurasian cold anomaly to the modulation of Ural blocking by ENSO. Geophys Res Lett. https://doi.org/10.1029/2021GL094304

Masato G, Hoskins BJ, Woollings TJ (2013) Wave-breaking characteristics of Northern Hemisphere winter blocking: a two-dimensional approach. J Clim 26:4535–4549

Meehl GA, Hu A, Castruccio F et al (2021) Atlantic and Pacific tropics connected by mutually interactive decadal-timescale processes. Nat Geosci 14:36–42

Mori M, Watanabe M, Shiogama H, Inoue J, Kimoto M (2014) Robust Arctic sea-ice influence on the frequent Eurasian cold winters in past decades. Nat Geosci 7:869–873. https://doi.org/10.1038/ngeo2277

Nakamura T, Yamazaki K, Iwamoto K, Honda M, Miyoshi Y, Ogawa Y, Tomikawa Y, Ukita J (2016) The stratospheric pathway for Arctic impacts on midlatitude climate. Geophys Res Lett 43:3494–3501

Power S, Casey T, Folland C, Colman A, Mehta V (1999) Interdecadal modulation of the impact of ENSO on Australia. Clim Dyn 15:319–324. https://doi.org/10.1007/s003820050284

Rayner NA, Parker DE, Horton EB, Folland CK, Alexander LV, Rowell DP, Kent EC, Kaplan A (2003) Global analyses of sea surface temperature, sea ice, and night marine air temperature since the late nineteenth century. J Geophys Res 108:4407. https://doi.org/10.1029/2002JD002670

Rimbu N, Lohmann G, Ionita M (2014) Interannual to multidecadal Euro-Atlantic blocking variability during winter and its relationship with extreme low temperatures in Europe. J Geophys Res 119:13621–13636. https://doi.org/10.1002/2014JD021983

Rudeva I, Simmonds I (2021) Midlatitude winter extreme temperature events and connections with anomalies in the Arctic and tropics. J Clim 34:3733–3749. https://doi.org/10.1175/JCLI-D-20-0371.1

Simmonds I, Li M (2021) Trends and variability in polar sea ice, global atmospheric circulations and baroclinicity. Ann NY Acad Sci. https://doi.org/10.1111/nyas.14673

Sung M-K, Kim S-H, Kim B-M, Choi Y-S (2018) Interdecadal variability of the Warm Arctic and Cold Eurasia Pattern and its North Atlantic origin. J Clim 31:5793–5810. https://doi.org/10.1175/JCLI-D-17-0562.1

Tibaldi S, Molteni F (1990) On the operational predictability of blocking. Tellus 42A:343–365. https://doi.org/10.1034/j.1600-0870.1990.t01-2-00003.x

Trenberth KE, Shea DJ (2006) Atlantic hurricanes and natural variability in 2005. Geophys Res Lett 33:L12704. https://doi.org/10.1029/2006GL026894

Tyrlis E, Bader J, Manzini E, Ukita J, Nakamura H, Matei D (2020) On the role of Ural Blocking in driving the Warm Arctic-Cold Central Eurasia pattern. Q J R Meteorol Soc 146:2138–2153

Wei M, Qiao F, Deng J (2015) A quantitative definition of global warming hiatus and 50-Year prediction of global-mean surface temperature. J Atmos Sci 72:3281–3289

Wilks DS (2011) Statistical methods in the atmospheric sciences, 3rd edn. Academic Press, Oxford

Woollings TJ, Hoskins BJ, Blackburn P, Berrisford P (2008) A new Rossby wave-breaking interpretation of the North Atlantic Oscillation. J Atmos Sci 65:609–626. https://doi.org/10.1175/2007JAS2347.1

Wu Z, Lin H (2012) Interdecadal variability of the ENSO-North Atlantic Oscillation connection in boreal summer. Q J R Meteorol Soc 138:1668–1675. https://doi.org/10.1002/qj.1889

Wu Z, Zhang P (2015) Interdecadal variability of the mega-ENSO–NAO synchronization in winter. Clim Dyn 45:1117–1128

Wyatt MG, Kravtsov S, Tsonis AA (2012) Atlantic Multidecadal Oscillation and Northern Hemisphere's climate variability. Clim Dyn 38:929–949

Yao Y, Luo D, Dai A, Simmonds I (2017) Increased quasi stationarity and persistence of winter Ural blocking and Eurasian extreme cold events in response to Arctic warming. Part I: insights from observational analyses. J Clim 30:3549–3568

Zhang R, Delworth TL (2007) Impact of the Atlantic multidecadal oscillation on North Pacific climate variability. Geophys Res Lett 34:L23708. https://doi.org/10.1029/2007GL031601

Zhang W, Luo D (2020) A Nonlinear theory of atmospheric blocking: an application to Greenland blocking changes linked to winter Arctic sea ice loss. J Atmos Sci 77:723–751

Zhou Y, Wu Z (2016) Possible impacts of mega-El Niño/Southern Oscillation and Atlantic Multidecadal Oscillation on Eurasian heatwave frequency variability. Q J R Meteorol Soc 142:1647–1661. https://doi.org/10.1002/qj.2759